Processing of Lake Baikal Marine Multichannel Seismic Reflection Data

by

D. R. Hutchinson[1], M. W. Lee[2], W. F. Agena[2], A. J. Golmshtok[3], V. N. Moskalenko[3], K. Karapetov[4], D. F. Coleman[1], L. Akentiev[3]

[1]U.S. Geological Survey, Woods Hole, MA 02543
[2]U.S. Geological Survey, Denver, CO 80225
[3]Southern Branch, Institute of Oceanology, Gelendzhik, Russia
[4]Irkutskgeophysica, Irkutsk, Russia

U. S. Geological Survey

Open-File Report 92-243

February, 1992

CONTENTS

INTRODUCTION

In summer, 1989, the former U.S.S.R. Academy of Sciences collected approximately 1500 km of marine multichannel seismic reflection data in Lake Baikal, south-central Siberia, as part of a multidisciplinary, international program of research to study the geodynamics, paleolimnology, and paleoclimatology of the lake. Lake Baikal is the deepest, largest by volume, and potentially the oldest of the Earth's fresh water lakes (Kozhov, 1963). It is 650 km long and occupies approximately one third of the Baikal rift zone, an active continental rift. The lake is divided into three basins, South, Central, and North, by two bathymetric sills, Selenga Delta and Academician Ridge (Fig. 1). The seismic profiles provide data from each of the basins (16 dip lines) as well as an axial strike line.

Lake Baikal poses challenges to the acquisition of seismic data: the freshwater reduces the buoyancy of the streamer; the extremely cold water affects the smooth operation of air guns; the deep water (in excess of 2 s two-way travel time) generates deep water multiples; and the poorly charted bathymetry makes navigation a hazard in some of the regions of rapidly changing water depths along the eastern shore of the lake. Preliminary processing showed that the biggest problem affecting the seismic data was the low-frequency content and resulting poor signal-to-noise ratios associated with the use of a single large air gun source. Low frequencies are often desireable for maximizing the penetration of the seismic signal in the Earth, at a cost of reduced resolution and signal quality.

In order to provide meaningful profiles for geological interpretation, particularly for outlining the structural and stratigraphic framework of the rift basins within the lake, we developed a processing scheme that would optimize the signal quality. This report describes the acquisition parameters and processing strategy we used to maximize the resolution and quality of the multichannel data.

ACKNOWLEDGEMENTS

The data acquisition was done entirely by the scientists of the former U.S.S.R. (now Russian) Academy of Sciences (Southern Branch of the Institute of Oceanology and Limnological Institute). We thank the Captain and crew of the R/V Balkhash for help during the acquisition phases. Special appreciation is extended to Dr. M. Grachev and V. Fialkov of the Limnological Institute for funding the ship time, obtaining the necessary permits to work in the lake and providing additional key personnel.

The processing was done at the U.S. Geological Survey by American and Russian scientists under a joint agreement of cooperative research between the respective scientific organizations. Processing was performed on a VAX 11/780 computer using Cogniseis DISCO software with additional programs developed by M.W. Lee of the U.S.G.S. We thank the Geophysics Group of the Branch of Petroleum Geology for their patience and expertise in accomodating busy schedules during the processing of these data.

We thank John Miller and Dave Foster for suggestions on improving this report.

DATA ACQUISITION

The Lake Baikal multichannel data consist of 17 lines (Figure 1) that were collected in July and August, 1989, aboard the R/V Balkhash using equipment owned and operated by the Limnological Institute (Irkutsk, Russia) and the Southern Branch of the Institute of Oceanology (Gelendzhik, Russia). The energy source consisted of a single 17-liter air gun (about 1000 cubic inches) towed at 15-m depth and shot on time intervals of 1 - 2 minutes to yield nominal 50-m or 100-m shot spacing. Only the axial line in the North basin (lines 15-1A, 15-1B) was shot with 100-m shot spacing. The receiver was a 1200-m long hydrophone streamer containing 24 channels spaced at 50-m intervals. This configuration gives 12-fold multiplicity for 50-m shots and 6-fold multiplicity for 100-m shots. The near offset was typically 400 m, but was increased to 450 m for most of the axial profile (line 15). The streamer, like the air gun, was towed at 15-m depth. For a distance of about 15 km on the axial line over Academician Ridge (line 15-1C), the streamer was not horizontal in the water: the tail end rose to the surface.

The data were recorded in on magnetic tape SEG-B format using a Soviet-built acquisition computer called a seismograph station. The record length was 7s with delays of 0 s, 1.024 s, and 2.048 s programmed according to water depth. The sample rate was 2 ms. The original field tapes were copied onto 185 1600-bpi tapes for shipment to the U.S. for processing. Minor data loss occurred during the copying. A summary of general information about the seismic lines is given in Table 1. Only one tape of line 4 could not be demultiplexed, resulting in a loss of 131 shots at the end of the line.

Navigation was by radar and dead reckoning, with fixes recorded about every 30 minutes. Figure 1 is a map of unannotated trackline locations. Plate 1 is a map of the track locations and navigation control points with shot points annotated. Appendix I is a list of the half-hour control points for the navigation. Intermediate shot points were determined by linear interpolation and extrapolation between the control points.

NOISE AND SIGNAL CHARACTERISTICS

Initial demultiplexing of the data revealed the cyclical, reverberative, and low-frequency character of the data. The unfiltered and filtered near traces of a portion of line 15-6 from the South basin are shown in Figure 2, and the amplitude spectrum of an individual trace from Figure 2 is shown in Figure 3. The dominant frequency is about 12.5 hz, and the spectrum is not flat. This frequency yields an effective quarter-wavelength resolution of 29 m for fresh water (1440 m/s). The quarter-wavelength resolution would be even worse for media with higher velocities (e.g., 80 m for 4000 m/s material). This is considered poor resolution for identifying small changes in stratigraphic thickness and depositional environment that one might expect to encounter in a large, closed basin such as Lake Baikal. One advantage of the low-frequency content of the signal is to allow the data to be resampled from 2 ms to 4 ms, thereby halving the volume of data to be processed.

A second problem with the data involved random static shifts of up to 20 ms for entire shot traces (Figure 4a). The typical shift was about 10 - 15 ms, i.e., more than a quarter wavelet shift for frequencies above 17 Hz. This shift therefore affects the range of frequencies of most interest in the data and could significantly degrade data quality

during stack of adjacent traces. Inspection of the data showed that the shifts almost always occurred when the gun firing delay was set to 1.024 s, suggesting that the firing circuit was somehow flawed when the 1.024-s delay was active. However, we cannot entirely eliminate the possibility that the cold water of the lake adversely affected the mechanical firing of the gun. These shifts were manually corrected with completely satisfactory results (Figure 4b).

Our third observation about the data involves the variable signal strength through the section, and in particular the strong multiple energy and the obvious loss of signal quality at the position of the first water-bottom multiple in deep water (more than 700 m or 1 s). Figure 5 is a brute stack of the data in which only a prestack automatic gain control (AGC) of 350 ms was applied prior to normal moveout, mute and stack. The dim spot or blanking at the level of the first multiple (3.8 s) is typical of the signal in deep water for all of the lines in this study. We cannot entirely rule out the possibility that the basin reflectivity coincidentally changes at the position of the first multiple, although we think such an occurrence is unlikely. A more likely explanation of the blanking is malfunction of the dynamic gain ranging in the recording system, causing the multiple energy to saturate the recording amplifiers.

Our final observation about the data is that the shape and duration of the source wavelet is quite consistent from shot to shot (Figure 6). We use this characteristic to justify performing wavelet deconvolution on the data in our processing strategy.

PROCESSING STRATEGY AND TESTS

The observations noted above emphasize the need to design the processing to maximize the resolution of the data, i.e., to mimimize the ringiness, to eliminate random jitter, and to bolster the signal-to-noise ratios in the section beneath the first multiple (primarily in deep water). Because the random jitter problem is a simple static shift, this step was performed as part of the routine editing of the data after demultiplexing. Our tests therefore focused on addressing the ringiness and signal-quality issues.

Signal reverberation: One of the easiest methods of improving the resolution and high-frequency content of the data is to perform a statistical deconvolution. We applied a spiking deconvolution algorithm after a 350-ms AGC to collapse the reverberative signal into a single pulse (Figure 7). The deconvolution operator was designed using a single window that included the water bottom and the first water-bottom multiple. The resulting operator was applied to the entire section, followed by a band pass filter of 5 to 70 Hz. This processing sequence did an adequate job of collapsing the reverberation, but the signal quality in the deeper section (5 to 7 s) is still poor.

Next, we tested a wavelet deconvolution algorithm (variable norm deconvolution; Gray, 1979) to improve the signal. This is justified because of the good repeatability of the source signal (Figure 6). A representative source signature is extracted from the data, and then an inverse filter is calculated and applied to all of the shots in each line. Model studies have shown that a representative source signature can be applied to the entire profile rather than applying a separate deconvolution filter to each gather (Dragoset and others, 1987). We tested two filters, one using a 400-ms design window, the second using

a 700-ms design window. Figure 8 gives the extracted wavelet and spectra for the 400-ms (panels a and c) and 700-ms (panels b and d) design windows. Figure 9 gives the filtered trace and spectra after wavelet deconvolution for the two design windows. Note that the water bottom is the large negative peak on each example. Figure 10 illustrates the ungained and AGC-gained near traces after application of each of the wavelet decon filters. The water bottom is the negative (unfilled) wavelet at 1.95 s. Both of the AGC-gained sections show a low-frequency precursor prior to the water bottom arrival, but the precursor on the 700-ms design filter is much less pronounced. The differences between the two filters are subtle. We chose to use the 700-ms design window because of the more subdued precursor to the water bottom.

A test of the stack with the wavelet decon filter based on the 700-ms design window followed by a 350-ms AGC is shown in Figure 11. A comparison of Figure 11 with Figures 5 (brute stack) and 7 (no wavelet processing) shows that the wavelet processing has effectively collapsed the wavelet and significantly improved the appearance and resolution of both the shallow (2-4 s) and deeper (5-7 s) sections.

Multiple suppression: In order to deemphasize the multiple energy, we tested a prestack predictive deconvoultion and weighted stack (in which the far traces are weighted more than the near traces during the stack). Weighted stacks are effective in regions of strong multiples when there are differences in moveout between the primary and multiple energy at the furthest offsets (Yilmaz, 1987). A section with predictive deconvolution but without weighted stack (Figure 12) can be compared to a similar section with weighted stack (Figure 13). This comparison shows that the weighted stack suppresses the first order multiples (at 3.8 s) effectively and slightly improves the signal strength in the deeper section (5 - 7 s). Comparing figures 11 and 13, we can observe that the predictive deconvolution suppresses the dispersed multiple energy (around 5.8 s) more effectively. The predictive deconvolution has a prediction distance of the first zero crossing of the autocorrelation of the data.

The final test we performed was to determine the effectiveness of spectral whitening instead of the prestack predictive deconvolution in the processing stream (Lee, 1986). For this test, the wavelet processing was followed by a 1000-ms AGC, amplitude balancing, spectral whitening, and then the weighted stack (Figure 14). Overall signal strength in this section is less than in Figure 13, due to the generally higher levels of background noise.

Our final strategy therefore follows the processing sequence used to generate Figure 13: prestack wavelet deconvolution followed by a moderate (350-ms) AGC, a predictive deconvolution with a short prediction distance, and a weighted stack. This strategy was most effective in collapsing the reverberative wavelet, improving the resolution of the data, and increasing the signal strength in the deeper portions of the profiles.

PROCESSING PRIOR TO MIGRATION

Figure 15 summarizes the steps used to process the Lake Baikal multichannel data. The initial editing proved to be tedious because of the need to manually pick and then apply the statics corrections for the shot jitter. Other editing involved deleting bad traces, applying the firing delay correction (0, 1.024, or 2.048 s), and renumbering shots due to miscounts in the demultiplexing procedure. Demultiplexed, edited data

are archived on 9-track magnetic tape in SEG-Y format (Appendix 2).

The wavelet deconvolution was applied to 8 s of data, and hence all record lengths were standardized at 8 s. This involved loss of 1 s of data in the deep-water regions of the lake where the actual data recording had been 2.048 - 9.048 s. Inspection of the (unprocessed) near trace data showed no arrivals other than multiple energy at travel times greater than 8 s.

Three to five iterations of velocity analysis were performed to ensure smooth and realistic velocities. Initial velocities were chosen from analyses that used seven trial time-varying velocity functions, and displayed both NMO-corrected unstacked and stacked traces. These RMS velocities were smoothed using either a gridding and moving average technique (lines 8 and 10; Miller, 1991) or along reflecting horizons by comparison with and smoothing of interval velocities calculated from stacking velocities. The final RMS velocities show no large lateral discontinuities, and interval velocities are also reasonably smooth (Figure 16), although they are not well constrained below about 2 s beneath the lake floor.

The RMS velocities were extremely low, generally from about 1390 to 1460 m/s at the lake floor, increasing to about 2000 m/s at 2 - 3 s subbottom in the deep sedimentary basins. Calculated interval velocities are also low within the resolved sedimentary section, generally less than 3.0 km/s. We estimate that the interval velocities are accurate to about 10 - 15 % at 3-4 s travel time in the deep basins.

Mute was applied after NMO and before the weighting for stack. All lines were archived to tape after stack and before final display. A list of the archived tapes is given in Appendix 3.

Post-stack processing: A predictive deconvolution operator was applied based on a prediction distance of the second zero crossing of the autocorrelation followed by a simple bandpass filter of 10 to 40 Hz. No post-stack AGC was applied because this only served to amplify the multiple energy. The stacked sections were displayed on mylar film and are archived by U.S.Geological Survey, Woods Hole, and Southern Branch of the Institute of Oceanology, Gelendzhik, Russia.

POST-STACK MIGRATION PROCESSING

Migration of the data was warranted because of the large relief changes in the morphology of the lake, the highly faulted sedimentary section, and the rapid changes in the thickness of the sediments. Eight of the dip lines were migrated, representing one of each pair of lines, except for the northernmost pair in the North basin. Five portions of the axial line that showed complex structure or convincing arrivals at 5 - 7 s (the observed level of the basement) were also migrated. A summary of the archived migrated tapes is given in Appendix 4.

Figure 15 illustrates the post-stack processing steps. In preparation for migration, two adjacent traces were summed to halve the volume of data being migrated. A second-zero crossing predictive deconvolution was then applied.

The migration technique used is called cascaded migration (Larner and Beasley, 1987; Beasley and others, 1988). First, a frequency-wavenumber migration was performed using either a constant velocity, that

of fresh water (1440 m/s), or a vertically varying velocity function having a low gradient. This served to effectively migrate the steep water-bottom arrivals, but the rest of the section was still undermigrated. It also served to eliminate most of the diffractions and occasional side-scattered noise in the profiles. In the second step, a finite-difference migration with small lateral and vertical residual velocity changes completed the migration of the sedimentary and basement section. Despite the numerically intensive calculations involved in migrating the data twice, this approach yields superior results because it combines the best features of both migrations: migrating steeply dipping events relatively fast (F-K migration) and accomodating lateral and vertical (residual) velocity variations at lower apparent dip (finite difference migration).

RESULTS AND DISCUSSION

Two lines illustrate the effectiveness and limitations of the data processing strategy: lines 8 and 6, both from the Central basin of Lake Baikal. Line 8 (Figure 17) is located along a north-south profile that begins at the south end of the North basin, crosses Academician Ridge, and continues across the Central basin just east of the deepest point in the lake. The data quality is considered to be excellent because inferred basement, the deepest identifiable reflector on any of the profiles, can be imaged almost continuously along the profile (Figure 17). Within the sedimentary section, many continuous reflections, seismic unconformities, and fault offsets occur at travel times up to 2 s beneath the lake floor. As on many other lines, blanking occurs at travel times greater than the first multiple in deep water (SP 1200 - SP 1800). The presence of a fairly strong basement reflection and occassional disrupted reflections within the deepest, blanked unit suggests that not all the source energy was overwhelmed by the multiple energy. That is, primary energy can be identified up to about 5 s beneath the lake floor. The distinct fading of reflections at the level of the first multiple indicated that our processing strategy did not entirely overcome this problem.

Line 6, from the north side of the Selenga Delta in the Central basin, shows an example of a profile where basement was not imaged anywhere on the profile, and short, disrupted reflector fragments with numerous diffractions characterize the sedimentary section (Figure 18). Blanking occurs at the level of the first multiple, and no primary reflection energy can be reliably identified beneath the first multiple, i.e., subbottom returns are limited to about 2 s beneath the lake floor. This same limited penetration phenomenon occurs on several strike and dip lines; it is always associated with short, disrupted reflections and diffractions within the sedimentary section. A possible interpretation of the much poorer signal quality on line 6 and these other lines is that the processing strategy did not work well. We prefer an alternative interpretation which is that the local geology is affecting the signal strength, and that the short, disrupted reflector segments originate from regions of sedimentary disruption and greater signal attenuation.

Although the overall quality of the multichannel data is good, the 1989 Baikal data contain some insurmountable limitations that the processing could not remedy. The source (single, large, air gun with a narrow spectral range) could be compensated for in the processing, but it inherently lacks the resolution of a more broadband source, such as arrays of smaller guns. The uncertainty in the dynamic range of the recording system is the most likely explanation for the blanking that

occurs at the level of the first multiple in deep water. If this narrow dynamic range did occur, then no amount of processing will recover data that were not initially recorded. The large uncertainty in navigation fixes, resulting in the need for firing the air gun on time rather than distance, introduces a spatial smearing into the data. This problem does not appear to be serious, given the overall continuity of reflections and reflection packages such as those on line 8. A more serious limitation of the navigation is that the profiles can not be used for detailed mapping and correlation. However, given the large line spacing (10 - 60 km) between adjacent lines, the data are best suited for a regional overview and interpretation.

The existing data image a wide range of complex structure and stratigraphy, which indicate the need for a much tighter grid of data to map fault geometry and depositional sequences.

CONCLUSIONS

(1) The major problems affecting the processing of the Baikal multichannel data were the low-frequency reverberative nature of the air-gun source signal, the random static shifts of up to 20 ms in the firing of the gun, and the blanking of the stacked data at the level of the first water-bottom multiple in deep water.

(2) Conventional processing, such as prestack AGC and spiking deconvolution, served to improve the resolution (i.e., increased bandwidth and reduced reverberations) of the data but failed to significantly improve the signal-to-noise ratios in the deeper section. Conventional static shifts did, however, correct the random static shift problem.

(3) Special prestack processing, involving the application of wavelet deconvolution followed by AGC and predictive deconvolution, provided the optimum processing flow for improving the resolution and signal strength of the data. In general, the images of the sedimentary section on the 17 profiles in the lake are good to excellent, although blanking could not totally be removed in the processing.

(4) Post-stack processing focused on migrating the data to restore geometric relations between reflections. A two-step cascading migration in which the data were initially migrated with an f-k algorithm using the velocity of water (or a vertically varying velocity function having a low gradient) followed by a finite difference algorithm using smoothed residual velocities, provided the most satisfactory migration of the steep morphology and dipping layers in the lake. Because most of the lines were collected as pairs, only one of each pair was migrated.

(5) Additional limitations of the data inherent in the acquisition were the spatial smearing due to firing the air gun on time rather than distance (a problem we judge to be relatively minor) and the navigational inaccuracy caused by half-hour radar and dead-reckoning fixes (a problem that most affects the interpretation of the data).

REFERENCES CITED

Beasley, C., Lynn, W., Larner, K., and Nguyen, H., 1988, Cascaded *f-k* migration: removing the restrictions on depth varying velocities: Geophysics, v. 53, p. 881 - 893.

Dragoset, B., Hargreaves, N., and Larner, K., 1987, Air-gun source instabilities: Geophysics, v. 52, p. 1229 - 1251.

Gray, W.C., 1979, Variable norm deconvolution: Palo Alto, CA, Stanford University Ph.D. thesis.

Kozhov, M., 1963, Lake Baikal and its life: Dr. W. Junk Publishers, the Hague, 344 pp.

Larner, K., and Beasley, C., 1987, Cascaded migrations: improving the accuracy of finite-difference migration: Geophysics, v. 52, p. 618-643.

Lee, M.W., 1986, Spectral whitening in the frequency domain: U.S. Geological Survey Open-file Report 86-108, 15 pp.

Miller, J.J., 1991, A VAX and MS-DOS computer program package for depth conversion of digitized line-drawing interpretations of seismic sections: U.S. Geological Survey Open-file Report 91-303A, 25 pp.

Yilmaz, O., 1987, Seismic data processing: Society of Exploration Geophysicists Investigations in Geophysics, v. 2, 526 p.

TABLE 1: GENERAL TRACKLINE INFORMATION

Line No.	Shot Interval	First Shot	Last Shot	Total Shots	Total Km
1	50-m	1	500	500	25.00
2	50-m	1	562	562	28.10
3	50-m	1	752	749	37.45
4	50-m	781	1372	469	23.45
5	50-m	1	541	541	27.05
6	50-m	1	626	626	31.30
7	50-m	815	2846	2031	101.55
8	50-m	315	2340	2025	101.25
9	50-m	847	2045	1198	59.90
10	50-m	1	1314	1314	65.70
11	50-m	1	1326	1326	66.30
12	50-m	1	1310	1310	65.50
13	50-m	1	661	661	33.05
14	50-m	1	593	593	29.65
15-1A	100-m	8152	9600	1449	144.90
15-1B	50-m 100-m	7427 7440	7439 8151	13 711	.65 71.10
15-1C	50-m	6471	7426	956	47.80
15-2	50-m	3332	6470	3139	156.95
15-3	50-m	2427	3331	905	45.25
15-4	50-m	963	2406	1443	72.15
15-5	50-m	1	962	962	48.10
15-6	50-m	1	1593	1593	79.65
16	50-m	1	814	814	40.70
17	50-m	1	798	798	39.90
TOTALS				26688	1442.40

APPENDIX 1: Navigation Control Points

LATITUDE	LONGITUDE	SHOT	TIME
*****	LINE 1	*****	
51D37.1'N	105D04.8'E	1	00:20
51D37.5'N	105D04.3'E	21	00:30
51D38.8'N	105D03.0'E	80	01:00
51D40.4'N	105D02.4'E	139	01:30
51D41.6'N	105D01.6'E	199	02:00
51D43.1'N	105D00.1'E	260	02:30
51D44.2'N	104D58.8'E	320	03:00
51D45.5'N	104D57.9'E	380	03:30
51D46.7'N	104D56.4'E	439	04:00
51D48.2'N	104D55.3'E	500	04:30
*****	LINE 2	*****	
51D50.4'N	105D01.4'E	1	14:04
51D49.0'N	105D01.9'E	54	14:30
51D47.0'N	105D02.4'E	115	15:00
51D46.0'N	105D03.7'E	175	15:30
51D44.4'N	105D05.1'E	244	16:05
51D42.0'N	105D05.5'E	294	16:30
51D41.9'N	105D06.7'E	353	17:00
51D40.2'N	105D08.7'E	413	17:30
51D38.8'N	105D10.7'E	473	18:00
51D37.5'N	105D11.9'E	532	18:30
51D36.8'N	105D12.5'E	562	18:45
*****	LINE 3	*****	
51D58.3'N	106D02.0'E	1	20:05
51D58.2'N	106D01.8'E	3	20:06
51D58.7'N	105D59.6'E	45	20:27
52D04.8'N	105D50.0'E	352	23:00
52D06.5'N	105D49.1'E	410	23:30
52D07.8'N	105D47.1'E	469	00:00
52D09.2'N	105D45.8'E	529	00:30
52D10.5'N	105D44.1'E	590	01:00
52D11.7'N	105D42.1'E	650	01:30
52D13.1'N	105D41.7'E	710	02:00
52D14.1'N	105D41.4'E	752	02:21
*****	LINE 4	*****	
52D14.6'N	105D43.5'E	781	02:35
52D14.0'N	105D44.0'E	798	02:45
52D12.7'N	105D45.8'E	856	03:15
52D12.0'N	105D46.6'E	885	03:30
52D10.2'N	105D47.7'E	946	04:00
52D08.8'N	105D48.8'E	1018	04:35
52D07.8'N	105D51.5'E	1070	05:00
52D06.4'N	105D54.1'E	1130	05:30
52D05.5'N	105D56.0'E	1188	06:00
52D04.3'N	105D59.5'E	1308	07:00
52D02.8'N	106D02.0'E	1370	07:30
52D02.7'N	106D02.1'E	1372	07:31
*****	LINE 5	*****	
52D42.4'N	106D34.3'E	1	06:00
52D41.5'N	106D35.0'E	32	06:15
52D40.9'N	106D36.2'E	61	06:30
52D40.6'N	106D38.0'E	120	07:00
52D39.3'N	106D39.8'E	180	07:30
52D36.7'N	106D41.5'E	241	08:00
52D36.4'N	106D42.4'E	261	08:10
52D35.6'N	106D43.6'E	302	08:30
52D34.2'N	106D44.9'E	360	09:00
52D33.2'N	106D47.0'E	420	09:30
52D31.6'N	106D48.0'E	480	10:00
52D30.4'N	106D49.4'E	511	10:15
52D30.0'N	106D50.5'E	541	10:30
*****	LINE 6	*****	
52D45.8'N	106D38.1'E	1	13:02
52D45.7'N	106D38.2'E	6	13:05
52D44.8'N	106D39.2'E	57	13:30
52D43.7'N	106D40.1'E	116	14:00
52D42.7'N	106D43.0'E	177	14:30
52D41.3'N	106D44.6'E	237	15:00
52D40.0'N	106D45.5'E	295	15:30
52D38.8'N	106D47.3'E	348	16:00
52D36.2'N	106D51.8'E	469	17:00
52D35.0'N	106D53.5'E	541	17:37
52D34.0'N	106D55.5'E	586	18:00
52D33.1'N	106D57.3'E	626	18:20
*****	LINE 7	*****	
52D47.8'N	107D53.3'E	815	11:35
52D48.5'N	107D53.4'E	835	11:45
52D49.8'N	107D53.0'E	875	12:05
52D51.0'N	107D53.0'E	925	12:30
52D52.5'N	107D53.1'E	984	13:00
52D54.7'N	107D53.5'E	1044	13:30
52D56.7'N	107D53.7'E	1103	14:00
52D58.2'N	107D53.8'E	1162	14:30
53D00.0'N	107D53.5'E	1220	15:00
53D01.2'N	107D53.8'E	1277	15:30
53D03.2'N	107D54.7'E	1336	16:00
53D04.8'N	107D54.6'E	1393	16:30
53D06.2'N	107D54.1'E	1452	17:00
53D08.6'N	107D54.4'E	1513	17:30
53D11.2'N	107D54.5'E	1632	18:30
53D13.3'N	107D55.2'E	1688	19:00
53D14.5'N	107D55.5'E	1747	19:30
53D16.8'N	107D56.2'E	1808	20:00
53D18.2'N	107D55.6'E	1867	20:30
53D19.5'N	107D55.5'E	1926	21:00
53D21.0'N	107D55.2'E	1985	21:30
53D22.6'N	107D54.6'E	2043	22:00
53D24.8'N	107D54.2'E	2101	22:30
53D26.2'N	107D54.0'E	2160	23:00
53D27.5'N	107D53.9'E	2218	23:30
53D29.1'N	107D54.0'E	2278	24:00
53D30.8'N	107D53.3'E	2337	00:30
53D32.2'N	107D53.2'E	2397	01:00
53D33.8'N	107D53.5'E	2457	01:30
53D35.5'N	107D52.3'E	2517	02:00
53D37.4'N	107D52.7'E	2577	02:30
53D38.7'N	107D54.0'E	2636	03:00
53D40.2'N	107D53.8'E	2697	03:30
53D41.8'N	107D53.8'E	2757	04:00
53D44.2'N	107D53.9'E	2816	04:30
53D45.1'N	107D54.5'E	2846	04:45
*****	LINE 8	*****	
53D47.7'N	108D02.1'E	315	04:38
53D46.7'N	108D02.3'E	361	05:00
53D42.2'N	108D01.4'E	509	06:15
53D39.6'N	108D01.2'E	608	07:04
53D38.4'N	108D01.5'E	658	07:30
53D37.2'N	108D01.4'E	718	08:00
53D35.2'N	108D01.5'E	778	08:30
53D33.6'N	108D01.1'E	838	09:00
53D31.9'N	108D00.6'E	897	09:30
53D29.6'N	108D01.1'E	957	10:00
53D27.9'N	108D01.8'E	1018	10:30
53D26.6'N	108D00.7'E	1078	11:00
53D24.6'N	108D01.0'E	1137	11:30
53D23.7'N	108D00.9'E	1197	12:00
53D22.5'N	108D00.3'E	1256	12:30
53D21.1'N	108D01.5'E	1314	13:00
53D19.3'N	108D01.2'E	1374	13:30
53D18.2'N	108D01.4'E	1433	14:00
53D16.9'N	108D01.7'E	1493	14:30
53D15.3'N	108D01.4'E	1553	15:00
53D13.6'N	108D01.9'E	1613	15:30
53D11.8'N	108D02.3'E	1673	16:00
53D09.4'N	108D02.7'E	1733	16:30
53D07.5'N	108D02.8'E	1792	17:00
53D06.4'N	108D02.6'E	1852	17:30
53D04.7'N	108D03.4'E	1912	18:00
53D03.2'N	108D03.7'E	1972	18:30

LATITUDE	LONGITUDE	SHOT	TIME
53D01.5'N	108D03.6'E	2032	19:00
52D59.7'N	108D03.1'E	2092	19:30
52D57.9'N	108D02.5'E	2152	20:00
52D56.4'N	108D02.1'E	2111	20:30
52D54.8'N	108D02.0'E	2270	21:00
52D53.3'N	108D02.1'E	2330	21:30
52D53.0'N	108D02.1'E	2340	21:35
*****	LINE 9	*****	
53d45.4'n	107d58.5'e	847	05:26
53d45.2'n	107d58.6'e	855	05:30
53d44.0'n	108d00.2'e	912	06:00
53d40.8'n	108d01.3'e	1030	07:00
53d39.5,n	108d03.1'e	1090	07:30
53d38.2'n	108d05.5'e	1150	08:00
53d37.0'n	108d07.7'e	1210	08:30
53d35.4'n	108d09.4'e	1270	09:00
53d33.9'n	108d11.0'e	1330	09:30
53d31.7'n	108d12.5'e	1390	10:00
53d29.8'n	108d15.0'e	1450	10:30
53d26.8'n	108d16.6'e	1565	11:00
53d25.5'n	108d18.4'e	1624	12:00
53d25.0'n	108d21.1'e	1684	12:30
53d23.7'n	108d21.8'e	1743	13:00
53d22.2'n	108d23.3'e	1803	13:30
53d20.7'n	108d25.3'e	1860	14:00
53d19.5'n	108d26.3'e	1917	14:30
53d18.2'n	108d28.6'e	1970	15:00
53d17.7'n	108d30.2'e	2016	15:20
53d17.3'n	108d31.4'e	2045	15:35
*****	LINE 10	*****	
53D20.0'N	108D36.2'E	1	16:55
53D20.3'N	108D35.8'E	11	17:00
53D21.1'N	108D34.9'E	71	17:30
53D22.2'N	108D34.0'E	131	18:00
53D23.4'N	108D32.7'E	190	18:30
53D24.4'N	108D31.2'E	240	19:00
53D25.6'N	108D30.0'E	300	19:30
53D26.7'N	108D28.6'E	358	20:00
53D28.0'N	108D26.8'E	415	20:30
53D29.7'N	108D24.8'E	470	21:00
53D30.4'N	108D23.0'E	529	21:30
53D31.8'N	108D21.5'E	590	22:00
53D33.2'N	108D19.9'E	648	22:30
53D35.0'N	108D18.5'E	722	23:07
53D36.6'N	108D17.5'E	767	23:30
53D37.5'N	108D17.4'E	808	23:50
53D38.3'N	108D17.0'E	828	24:00
53D39.3'N	108D15.1'E	886	00:30
53D40.7'N	108D13.6'E	946	01:00
53D41.9'N	108D12.6'E	1006	01:30
53D43.4'N	108D11.3'E	1066	02:00
53D44.2'N	108D09.5'E	1126	02:30
53D45.8'N	108D08.1'E	1185	03:00
53D47.2'N	108D06.5'E	1246	03:30
53D48.1'N	108D06.0'E	1276	03:45
53D48.7'N	108D04.8'E	1305	04:00
53D48.7'N	108D04.1'E	1314	04:05
*****	LINE 11	*****	
54D06.2'N	109D27.1'E	1	18:00
54D06.4'N	109D25.8'E	31	18:15
54D06.7'N	109D24.8'E	61	18:30
54D06.9'N	109D22.0'E	121	19:00
54D07.0'N	109D19.0'E	190	19:35
54D07.5'N	109D16.5'E	240	20:00
54D08.0'N	109D14.1'E	300	20:30
54D08.8'N	109D10.6'E	359	21:00
54D09.1'N	109D10.0'E	419	21:30
54D09.8'N	109D07.8'E	479	22:00
54D10.7'N	109D05.0'E	539	22:30
54D10.9'N	109D02.5'E	599	23:00
54D11.3'N	108D59.5'E	659	23:30

LATITUDE	LONGITUDE	SHOT	TIME
54D11.8'N	108D57.0'E	719	24:00
54D12.5'N	108D54.6'E	779	00:30
54D13.1'N	108D52.1'E	839	01:00
54D13.6'N	108D49.1'E	899	01:30
54D13.9'N	108D46.7'E	959	02:00
54D14.5'N	108D44.5'E	1022	02:32
54D15.3'N	108D42.5'E	1078	03:00
54D15.5'N	108D39.8'E	1138	03:30
54D16.0'N	108D37.3'E	1198	04:00
54D16.5'N	108D34.6'E	1258	04:30
54D17.3'N	108D32.2'E	1318	05:00
54D17.4'N	108D31.9'E	1326	05:04
*****	LINE 12	*****	
54D21.7'N	108D33.6'E	1	05:30
54D20.0'N	108D37.7'E	89	06:15
54D19.5'N	108D38.7'E	117	06:30
54D19.4'N	108D41.4'E	177	07:00
54D18.5'N	108D42.0'E	206	07:15
54D18.4'N	108D43.4'E	234	07:30
54D18.0'N	108D46.5'E	300	08:05
54D17.9'N	108D49.7'E	350	08:30
54D17.9'N	108D51.4'E	410	09:00
54D17.8'N	108D53.6'E	470	09:30
54D17.1'N	108D56.8'E	529	10:00
54D16.3'N	108D59.5'E	589	10:30
54D15.5'N	109D01.2'E	649	11:00
54D15.3'N	109D03.6'E	709	11:30
54D13.8'N	109D06.2'E	768	12:00
54D13.8'N	109D08.5'E	827	12:30
54D12.4'N	109D11.8'E	887	13:00
54D11.5'N	109D12.7'E	917	13:15
54D11.4'N	109D15.0'E	967	13:40
54D11.0'N	109D16.4'E	1007	14:00
54D11.2'N	109D18.2'E	1037	14:15
54D11.1'N	109D20.0'E	1066	14:30
54D10.6'N	109D22.5'E	1096	15:00
54D10.1'N	109D25.8'E	1187	15:30
54D09.7'N	109D27.7'E	1245	16:00
54D09.3'N	109D29.7'E	1310	16:32
*****	LINE 13	*****	
55D26.3'N	109D45.4'E	1	03:40
55D26.5'N	109D45.0'E	11	03:45
55D27.0'N	109D43.8'E	40	04:00
55D27.6'N	109D41.5'E	100	04:30
55D28.0'N	109D39.0'E	159	05:00
55D28.6'N	109D36.5'E	218	05:30
55D29.3'N	109D34.0'E	278	06:00
55D29.3'N	109D34.0'E	346	06:34
55D30.0'N	109D31.0'E	398	07:00
55D31.3'N	109D26.5'E	456	07:30
55D31.9'N	109D23.6'E	528	08:06
55D32.3'N	109D21.7'E	575	08:30
55D32.6'N	109D19.4'E	628	09:00
55D32.8'N	109D18.1'E	646	09:10
55D33.2'N	109D17.5'E	661	09:18
*****	LINE 14	*****	
55D34.9'N	109D22.8'E	1	11:00
55D34.6'N	109D25.5'E	64	11:30
55D34.4'N	109D26.6'E	93	11:45
55D34.2'N	109D28.0'E	126	12:00
55D33.7'N	109D31.1'E	187	12:30
55D32.7'N	109D33.1'E	254	13:00
55D32.4'N	109D36.1'E	320	13:30
55D31.8'N	109D38.8'E	381	14:00
55D30.8'N	109D40.8'E	442	14:30
55D30.5'N	109D43.8'E	503	15:00
55D29.8'N	109D46.0'E	553	15:25
55D29.2'N	109D47.7'E	593	15:45
*****	LINE 15-1AB	*****	
54D30.2'N	108D59.5'E	8152	04:00
54D32.5'N	109D00.0'E	8185	04:30

LATITUDE	LONGITUDE	SHOT	TIME
54D33.4'N	109D01.4'E	8218	05:00
54D34.3'N	109D02.0'E	8251	05:30
54D35.2'N	109D03.1'E	8283	06:00
54D37.4'N	109D04.6'E	8316	06:30
54D38.8'N	109D05.0'E	8348	07:00
54D40.7'N	109D06.6'E	8383	07:30
54D42.5'N	109D07.6'E	8413	08:00
54D44.2'N	109D08.0'E	8444	08:30
54D46.0'N	109D09.5'E	8474	09:00
54D47.3'N	109D10.5'E	8505	09:30
54D48.9'N	109D11.3'E	8537	10:00
54D50.7'N	109D12.3'E	8568	10:30
54D52.8'N	109D13.0'E	8607	11:07
54D54.0'N	109D13.9'E	8633	11:30
54D55.7'N	109D14.5'E	8665	12:00
54D57.8'N	109D15.3'E	8697	12:30
54D59.5'N	109D15.8'E	8730	13:00
55D01.1'N	109D17.1'E	8768	13:35
55D02.9'N	109D18.0'E	8796	14:00
55D04.8'N	109D18.2'E	8829	14:30
55D06.3'N	109D18.8'E	8862	15:00
55D07.6'N	109D19.5'E	8895	15:30
55D09.5'N	109D20.3'E	8927	16:00
55D11.3'N	109D20.4'E	8960	16:30
55D12.6'N	109D22.1'E	8993	17:00
55D14.0'N	109D23.6'E	9025	17:30
55D15.3'N	109D24.9'E	9058	18:00
55D16.9'N	109D25.5'E	9090	18:30
55D18.5'N	109D26.6'E	9123	19:00
55D20.2'N	109D27.5'E	9156	19:30
55D21.1'N	109D28.9'E	9190	20:00
55D22.7'N	109D30.2'E	9222	20:30
55D25.0'N	109D32.0'E	9254	21:00
55D26.2'N	109D32.1'E	9286	21:30
55D27.6'N	109D32.7'E	9318	22:00
55D29.5'N	109D34.2'E	9351	22:30
55D31.0'N	109D35.2'E	9384	23:00
55D32.6'N	109D34.6'E	9417	23:30
55D34.2'N	109D35.9'E	9450	24:00
55D36.1'N	109D36.6'E	9472	00:30
55D38.2'N	109D37.6'E	9503	01:00
55D40.0'N	109D38.4'E	9535	01:30
55D41.0'N	109D39.0'E	9565	02:00
55D42.1'N	109D39.8'E	9585	02:20
55D42.9'N	109D40.0'E	9594	02:30
53D56.3'N	108D28.6'E	7427	17:00
53D58.2'N	108D28.4'E	7450	17:20
53D59.1'N	108D30.3'E	7492	18:00
54D00.6'N	108D30.4'E	7529	18:35
54D01.5'N	108D30.3'E	7553	19:00
54D03.8'N	108D33.2'E	7592	19:36
54D04.8'N	108D35.2'E	7619	20:00
54D05.6'N	108D36.3'E	7633	20:15
54D06.8'N	108D37.4'E	7649	20:30
54D07.7'N	108D38.4'E	7673	20:50
54D08.7'N	108D39.2'E	7685	21:00
54D09.6'N	108D40.6'E	7717	21:30
54D10.8'N	108D41.3'E	7753	22:00
54D12.5'N	108D43.1'E	7785	22:30
54D13.8'N	108D44.2'E	7820	23:00
54D15.1'N	108D45.9'E	7852	23:30
54D16.2'N	108D47.0'E	7884	24:00
54D18.3'N	108D48.5'E	7915	00:30
54D19.8'N	108D50.0'E	7949	01:00
54D21.5'N	108D51.0'E	7984	01:30
54D22.9'N	108D52.5'E	8002	01:45
54D23.8'N	108D53.8'E	8022	02:00
54D25.3'N	108D55.0'E	8056	02:30
54D26.8'N	108D56.5'E	8088	03:00
54D28.3'N	108D57.8'E	8120	03:30
54D30.2'N	108D59.5'E	8152	04:00

LATITUDE	LONGITUDE	SHOT	TIME
*****	LINE 15-1C	*****	
53D29.7'N	108D26.2'E	6471	08:45
53D32.0'N	108D26.7'E	6551	09:30
53D32.9'N	108D27.3'E	6580	09:45
53D35.5'N	108D27.5'E	6608	10:00
53D34.4'N	108D27.8'E	6632	10:12
53D35.4'N	108D28.1'E	6673	10:32
53D36.7'N	108D28.0'E	6726	11:00
53D38.3'N	108D28.4'E	6783	11:30
53D40.0'N	108D28.0'E	6835	12:00
53D41.4'N	108D28.5'E	6895	12:30
53D42.9'N	108D28.6'E	6952	13:00
53D44.7'N	108D28.7'E	7010	13:30
53D46.4'N	108D29.1'E	7067	14:00
53D48.5'N	108D29.2'E	7138	14:35
53D50.3'N	108D28.6'E	7186	15:00
53D51.7'N	108D29.2'E	7246	15:30
53D53.2'N	108D28.7'E	7306	16:00
53D54.7'N	108D27.6'E	7366	16:30
53D56.3'N	108D28.6'E	7427	17:00
*****	LINE 15-2	*****	
52D40.0'N	106D42.7'E	3332	05:30
52D41.0'N	106D44.5'E	3390	06:00
52D41.2'N	106D46.7'E	3447	06:30
52D42.3'N	106D49.4'E	3505	07:00
52D43.0'N	106D51.2'E	3564	07:30
52D44.6'N	106D55.0'E	3633	08:05
52D45.0'N	106D56.5'E	3683	08:30
52D45.5'N	106D57.0'E	3743	09:00
52D46.1'N	106D59.4'E	3803	09:30
52D47.1'N	107D01.2'E	3862	10:00
52D48.5'N	107D03.1'E	3922	10:30
52D49.5'N	107D04.7'E	3981	11:00
52D50.5'N	107D06.1'E	4040	11:30
52D51.6'N	107D07.9'E	4098	12:00
52D52.5'N	107D09.4'E	4158	12:30
52D53.5'N	107D11.7'E	4218	13:00
52D54.6'N	107D13.4'E	4277	13:30
52D55.0'N	107D15.0'E	4335	14:00
52D55.8'N	107D17.2'E	4393	14:30
52D56.5'N	107D20.3'E	4448	15:00
52D57.3'N	107D21.8'E	4505	15:30
52D58.1'N	107D23.8'E	4562	16:00
52D59.3'N	107D26.4'E	4606	16:30
53D00.5'N	107D29.3'E	4670	17:00
53D01.4'N	107D30.0'E	4725	17:30
53D02.7'N	107D32.3'E	4783	18:00
53D04.1'N	107D33.7'E	4876	18:46
53D04.7'N	107D33.8'E	4902	19:00
53D05.1'N	107D34.7'E	4962	19:30
53D06.2'N	107D36.0'E	5017	20:00
53D06.8'N	107D38.6'E	5100	20:45
53D06.8'N	107D39.9'E	5129	21:00
53D07.2'N	107D41.2'E	5157	21:15
53D07.7'N	107D41.9'E	5186	21:30
53D08.4'N	107D43.9'E	5236	22:00
53D09.0'N	107D45.2'E	5286	22:30
53D09.7'N	107D47.4'E	5340	23:00
53D11.1'N	107D50.0'E	5394	23:30
53D12.0'N	107D51.7'E	5450	24:00
53D12.8'N	107D54.2'E	5505	00:30
53D14.1'N	107D56.2'E	5564	01:00
53D14.6'N	107D58.3'E	5624	01:30
53D15.4'N	108D00.1'E	5683	02:00
53D17.1'N	108D02.3'E	5742	02:30
53D17.9'N	108D04.6'E	5800	03:00
53D19.3'N	108D06.4'E	5859	03:30
53D20.1'N	108D08.7'E	5916	04:00
53D20.8'N	108D10.7'E	5976	04:30
53D21.8'N	108D12.9'E	6035	05:30
53D22.8'N	108D15.7'E	6092	05:30

LATITUDE	LONGITUDE	SHOT	TIME
53D23.7'N	108D17.2'E	6150	06:00
53D24.7'N	108D19.3'E	6208	06:30
53D27.3'N	108D25.2'E	6384	08:00
53D29.7'N	108D26.2'E	6471	08:45
*****	LINE 15-3	*****	
52D28.0'N	106D09.3'E	2427	21:55
52D28.2'N	106D09.4'E	2437	22:00
52D28.5'N	106D10.3'E	2457	22:10
52D29.3'N	106D12.2'E	2497	22:30
52D29.4'N	106D13.3'E	2557	23:00
52D30.4'N	106D15.8'E	2616	23:30
52D31.0'N	106D17.2'E	2676	24:00
52D32.0'N	106D19.5'E	2736	00:30
52D32.7'N	106D22.0'E	2796	01:00
52D33.5'N	106D25.0'E	2855	01:30
52D34.7'N	106D27.1'E	2915	02:00
52D35.3'N	106D28.3'E	2974	02:30
52D36.0'N	106D31.1'E	3034	03:00
52D36.7'N	106D33.0'E	3093	03:30
52D37.3'N	106D35.7'E	3153	04:00
52D37.8'N	106D37.5'E	3213	04:30
52D39.0'N	106D39.7'E	3273	05:00
*****	LINE 15-4	*****	
51D55.1'N	105D31.5'E	963	09:30
51D56.3'N	105D33.0'E	1018	10:00
51D57.7'N	105D34.6'E	1074	10:30
51D58.9'N	105D36.0'E	1128	11:00
52D00.2'N	105D37.5'E	1184	11:30
52D01.8'N	105D38.9'E	1244	12:00
52D03.9'N	105D41.3'E	1302	12:30
52D05.0'N	105D42.2'E	1362	13:00
52D05.8'N	105D43.2'E	1423	13:30
52D07.4'N	105D45.7'E	1483	14:00
52D08.8'N	105D47.3'E	1543	14:30
52D10.4'N	105D49.1'E	1603	15:00
52D12.0'N	105D50.8'E	1664	15:30
52D13.9'N	105D52.5'E	1723	16:00
52D15.5'N	105D53.8'E	1795	16:35
52D17.0'N	105D54.8'E	1847	17:00
52D18.3'N	105D55.7'E	1908	17:30
52D19.8'N	105D58.0'E	1968	18:00
52D21.0'N	105D59.4'E	2026	18:30
52D21.6'N	106D00.4'E	2056	18:45
52D21.8'N	106D01.4'E	2086	19:00
52D22.8'N	106D02.4'E	2146	19:30
52D23.7'N	106D04.2'E	2205	20:00
52D24.8'N	106D06.0'E	2266	20:30
52D25.7'N	106D07.4'E	2326	21:00
52D27.1'N	106D08.6'E	2386	21:30
52D27.5'N	106D08.9'E	2406	21:40
*****	LINE 15-5	*****	
51D41.5'N	104D53.8'E	1	01:15
51D42.7'N	104D58.1'E	90	02:00
51D43.3'N	105D00.2'E	149	02:30
51D44.0'N	105D03.2'E	208	03:00
51D44.2'N	105D06.3'E	268	03:30
51D45.2'N	105D08.3'E	329	04:00
51D46.7'N	105D10.0'E	394	04:30
51D47.0'N	105D13.4'E	456	05:00
51D47.9'N	105D14.8'E	516	05:30
51D49.0'N	105D16.8'E	575	06:00
51D49.6'N	105D18.9'E	635	06:30
51D50.3'N	105D20.8'E	694	07:00
51D51.2'N	105D22.3'E	754	07:30
51D52.2'N	105D24.1'E	812	08:00
51D53.2'N	105D27.3'E	872	08:30
51D53.9'N	105D28.9'E	932	09:00
51D54.5'N	105D30.5'E	936	09:15
51D55.1'N	105D31.5'E	963	09:30
*****	LINE 15-6	*****	
51D41.9'N	104D56.0'E	1	22:07
51D41.8'N	104D54.4'E	44	22:30
51D41.9'N	104D52.8'E	104	23:00
51D41.8'N	104D50.3'E	164	23:30
51D41.8'N	104D47.9'E	224	24:00
51D41.8'N	104D45.1'E	284	00:30
51D42.0'N	104D42.0'E	344	01:00
51D41.8'N	104D39.8'E	404	01:30
51D41.8'N	104D38.0'E	464	02:00
51D41.8'4	104D35.0'E	524	02:30
51D41.8'N	104D32.2'E	583	03:00
51D41.8'N	104D30.2'E	641	03:30
51D41.8'N	104D26.7'E	700	04:00
51D41.5'N	104D24.0'E	758	04:30
51D41.5'N	104D21.5'E	818	05:00
51D41.5'N	104D18.8'E	877	05:30
51D41.2'N	104D15.8'E	937	06:00
51D41.2'N	104D12.6'E	995	06:30
51D41.4'N	104D10.0'E	1053	07:00
51D41.0'N	104D08.2'E	1110	07:30
51D40.9'N	104D04.5'E	1168	08:00
51D40.8'N	104D02.1'E	1226	08:30
51D41.0'N	104D00.4'E	1285	09:00
51D41.1'N	103D58.4'E	1345	09:30
51D41.2'N	103D56.1'E	1400	10:00
51D41.3'N	103D53.6'E	1457	10:30
51D41.4'N	103D51.4'E	1514	11:00
51D41.3'N	103D48.9'E	1574	11:30
51D41.4'N	103D48.3'E	1593	11:40
*****	LINE 16	*****	
53D03.7'N	107D25.3'E	1	04:25
53D02.7'N	107D26.2'E	29	04:40
53D01.7'N	107D27.5'E	67	05:00
53D00.8'N	107D29.5'E	127	05:30
52D58.3'N	107D35.0'E	277	06:45
52D55.7'N	107D38.3'E	366	07:30
52D54.3'N	107D40.3'E	424	08:00
52D53.3'N	107D42.0'E	484	08:30
52D52.7'N	107D44.0'E	544	09:00
52D51.0'N	107D46.4'E	625	09:40
52D50.2'N	107D47.6'E	666	10:00
52D49.1'N	107D49.4'E	725	10:30
52D47.5'N	107D50.7'E	784	11:00
52D47.0'N	107D51.5'E	804	11:10
52D46.9'N	107D51.9'E	814	11:15
*****	LINE 17	*****	
52D50.7'N	107D57.2'E	1	22:42
52D51.0'N	107D57.0'E	10	22:46
52D53.2'N	107D55.7'E	67	23:15
52D53.3'N	107D54.7'E	96	23:30
52D54.8'N	107D52.7'E	155	24:00
52D55.5'N	107D50.1'E	214	00:30
52D57.0'N	107D47.9'E	273	01:00
52D58.1'N	107D46.6'E	333	01:30
52D59.1'N	107D44.5'E	393	02:00
53D00.7'N	107D42.5'E	451	02:30
53D02.0'N	107D40.9'E	509	03:00
53D02.8'N	107D39.7'E	567	03:30
53D03.9'N	107D37.7'E	623	04:00
53D05.0'N	107D36.5'E	699	04:40
53D06.4'N	107D33.4'E	735	05:00
53D06.7'N	107D32.8'E	754	05:10
53D07.8'N	107D32.0'E	792	05:30
53D08.0'N	107D32.0'E	798	05:33

APPENDIX 2: Tape Archive Information - Demultiplexed Data

Note: All archived data are in SEG-Y format. Shot ID is 2 bytes long starting at byte 189 of the trace header. Slot number is the U.S. Geological Survey identifier for the tape in the data base and in the tape library.

LAKE BAIKAL MULTICHANNEL DEMULTIPLEXED DATA - ARCHIVED

LINE NO.	SLOT NO.	REEL ID	START SHOT/TRACE	END SHOT/TRACE
1	4160 4161	B1D-1 B1D-2	1/1 410/7	410/6 502/24
2	4162 4163	B2D-1 B2D-2	1/1 410/17	410/16 548/24
3	4164 4165	B3D-1 B3D-2	1/1 412/12	412/11 752/24
4	4166 4167	B4D-1 B4D-2	754/1 1181/15	1181/14 1242/24
5	4168 4169	B5D-1 B5D-2	1/1 432/16	432/15 564/24
6	4188 4189	B6D-1 B6D-2	1/1 408/5	408/4 626/24
7	4329 4330 4331 4332 4333 4334	B7D-1 B7D-2 B7D-3 B7D-4 B7D-5 B7D-6	815/1 1184/2 1550/21 1927/21 2297/20 2703/3	1184/1 1550/20 1927/20 2297/19 2703/2 2846/24
8	4170 4171 4172 4173 4174 4175	B8D-1 B8D-2 B8D-3 B8D-4 B8D-5 B8D-6	315/1 682/13 1055/18 1391/22 1755/16 2119/4	682/12 1055/17 1391/21 1755/15 2119/3 2340/24
9	4335 4336 4337 4338	B9D-1 B9D-2 B9D-3 B9D-4	847/1 1212/3 1582/18 1954/17	1212/2 1582/17 1954/16 2042/24
10	4176 4177 4178 4179 4180	B10D-1 B10D-2 B10D-3 B10D-4 B10D-5	3/1 28/6 392/19 760/13 1129/8	28/5 392/18 760/12 1129/7 1314/24
11	6459 6460 6461 6462	B11D-1 B11D-2 B11D-3 B11D-4	1/1 412/16 823/2 1232/21	412/15 823/1 1232/20 1329/24
12	6463 6464 6465 6466	B12D-1 B12D-2 B12D-3 B12D-4	1/1 409/13 817/23 1226/23	409/12 817/22 1226/22 1310/24
13	6467 6468	B13D-1 B13D-2	1/1 410/18	410/17 661/24

LINE NO.	SLOT NO.	REEL ID	START SHOT/TRACE	END SHOT/TRACE
14	6469	B14D-1	1/1	412/11
	6470	B14D-2	412/12	593/24
15-1AB	4291	151ABD-1	7427/1	7831/3
	4292	151ABD-2	7831/4	8234/24
	4293	151ABD-3	8235/1	8644/8
	4294	151ABD-4	8644/9	8985/12
	4295	151ABD-5	8985/13	9394/18
	4296	151ABD-6	9394/19	9586/24
15-1C	4297	B151CD-1	6391/1	6798/24
	4298	B151CD-2	6799/1	7199/10
	4299	B151CD-3	7199/11	7427/24
15-2	4300	B152D-1	3332/1	3701/7
	4301	B152D-2	3701/8	4070/23
	4302	B152D-3	4070/24	4440/9
	4303	B152D-4	4440/10	4809/12
	4304	B152D-5	4809/13	5183/17
	4305	B152D-6	5183/18	5552/14
	4306	B152D-7	5552/15	5915/12
	4307	B152D-8	5915/13	6285/18
	4308	B152D-9	6285/19	6528/24
15-3	4309	B153D-1	2277/1	2686/23
	4310	B153D-2	2686/24	3101/6
	4311	B153D-3	3101/7	3357/24
15-4	4312	B154D-1	987/1	1397/6
	4313	B154D-2	1397/7	1799/9
	4314	B154D-3	1799/10	2209/14
	4315	B154D-4	2209/15	2276/24
15-5	7190	B155D-1	2/1	411/15
	7191	B155D-2	411/16	814/5
	7192	B155D-3	814/6	986/24
15-6	7193	B156D-1	1/1	410/9
	7194	B156D-2	410/10	820/9
	7195	B156D-3	820/10	1229/13
	7196	B156D-4	1229/14	1593/24
16	6471	B16D-1	1/1	369/16
	6472	B16D-2	369/17	732/11
	6473	B16D-3	732/12	814/24
17	4288	B17D-1	1/1	369/22
	4289	B17D-2	369/23	738/15
	4290	B17D-3	738/16	797/24

APPENDIX 3: Tape Archive Information - Stacked Data

NOTE: All data are in SEG-Y format. Shot ID is 2 bytes long starting at byte 189 of the trace header. Slot number is the U.S. Geological identifier for the tape in the data base and in the library.

LAKE BAIKAL STACKED DATA - ARCHIVED				
LINE NO.	SLOT	REEL ID	SHOTS START/END	CDPS START/END
1	13452	B1-1	1 - 498	1 - 1026
2	13453	B2-1	1 - 544	1 - 1118
3	13454	B3-1	1 - 748	1 - 1526
4	13455	B4-1	754 - 1238	1 - 2506
5	13456	B5-1	1 - 560	1 - 1150
6	13457	B6-1	1 - 622	1 - 1274
7	13458	B7-1	815 - 2828	1 - 4058
8	13459	B8-1	315 - 2336	1 - 4074
9	13460	B9-1	847 - 2041	1 - 2420
10	13461	B10-1	1 - 1310	1 - 2650
11	13462	B11-1	1 - 1325	1 - 2680
12	13463	B12-1	1 - 1306	1 - 2642
13	13464	B13-1	1 - 657	1 - 1344
14	13465	B14-1	1 - 589	1 - 1208
15-1AB	13466	B151AB-1	7427 - 9583	1 - 8634
15-1C	13457	B151C-1	6421 - 7422	1 - 2036
15-2	13468	B152-1	3332 - 6516	33 - 6434
15-3	13469	B153-1	2277 - 3352	885 - 3068
15-4	13470	B154-1	987 - 2271	280 - 2881
15-5	13471	B155-1	1 - 981	3 - 1994
15-6	13472	B156-1	1 - 1588	1 - 3208
16	13473	B16-1	1 - 809	1 - 1650
17	13474	B17-1	1 - 792	1 - 1614

APPENDIX 4: Tape Archive Information - Migrated Data

NOTE: All data are in SEG-Y format. Shot ID is 2 bytes long starting at byte 189 of the trace header. Slot number is the U.S. Geological Sruvey identifier for the tape in the data base and in the tape library.

LAKE BAIKAL MIGRATED DATA - ARCHIVED				
LINE NO.	SLOT	REEL ID	SHOTS START/END	CDPS START/END
1	13427	B1M-1	1 - 498	1 - 1025
2	13428	B2M-1	1 - 544	1 - 1117
3	13429	B3M-1	1 - 748	1 - 1525
4	13430	B4M-1	754 - 1238	1507 - 2505
5	13431	B5M-1	1 - 560	1 - 1149
6	13432	B6M-1	1 - 622	1 - 1273
7	13433	B7M-1	815 - 2828	1 - 4057
8	13434	B8M-1	315 - 2336	1 - 4073
9	13435	B9M-1	847 - 2041	1 - 2419
10	13436	B10M-1	1 - 1310	1 - 2649
11	13437	B11M-1	1 - 1325	1 - 2679
12	13438	B12M-1	1 - 1306	1 - 2641
13	13439	B13M-1	1 - 657	1 - 1343
14	13440	B14M-1	1 - 589	1 - 1207
15-1A	13441	B15ABM-1	7700 - 8000	1100 - 2300
15-1B	13442	B151AB-2	9300 - 9583	7500 - 8634
15-1C	13443	B151CM-1	6421 - 7422	1 - 2035
15-2	13444	B152M-1	3332 - 4065	33 - 1532
15-2	13445	B152M-2	5500 - 6500	4401 - 6402
15-3	13446	B153M-1	2277 - 3352	885 - 3067
15-4	13447	B154M-1	987 - 2271	280 - 2881
15-5	13448	B155M-1	1 - 981	3 - 1993
15-6	13449	B156M-1	1 - 1588	1 - 3207
16	13450	B16M-1	1 - 809	1 - 1649
17	13451	B17M-1	1 - 792	1 - 1613

Figure 1: Map showing the bathymetry and locations of the multichannel seismic reflection profiles in Lake Baikal. An enlarged version of this map with shot-point annotations and navigation control points is shown in Plate 1.

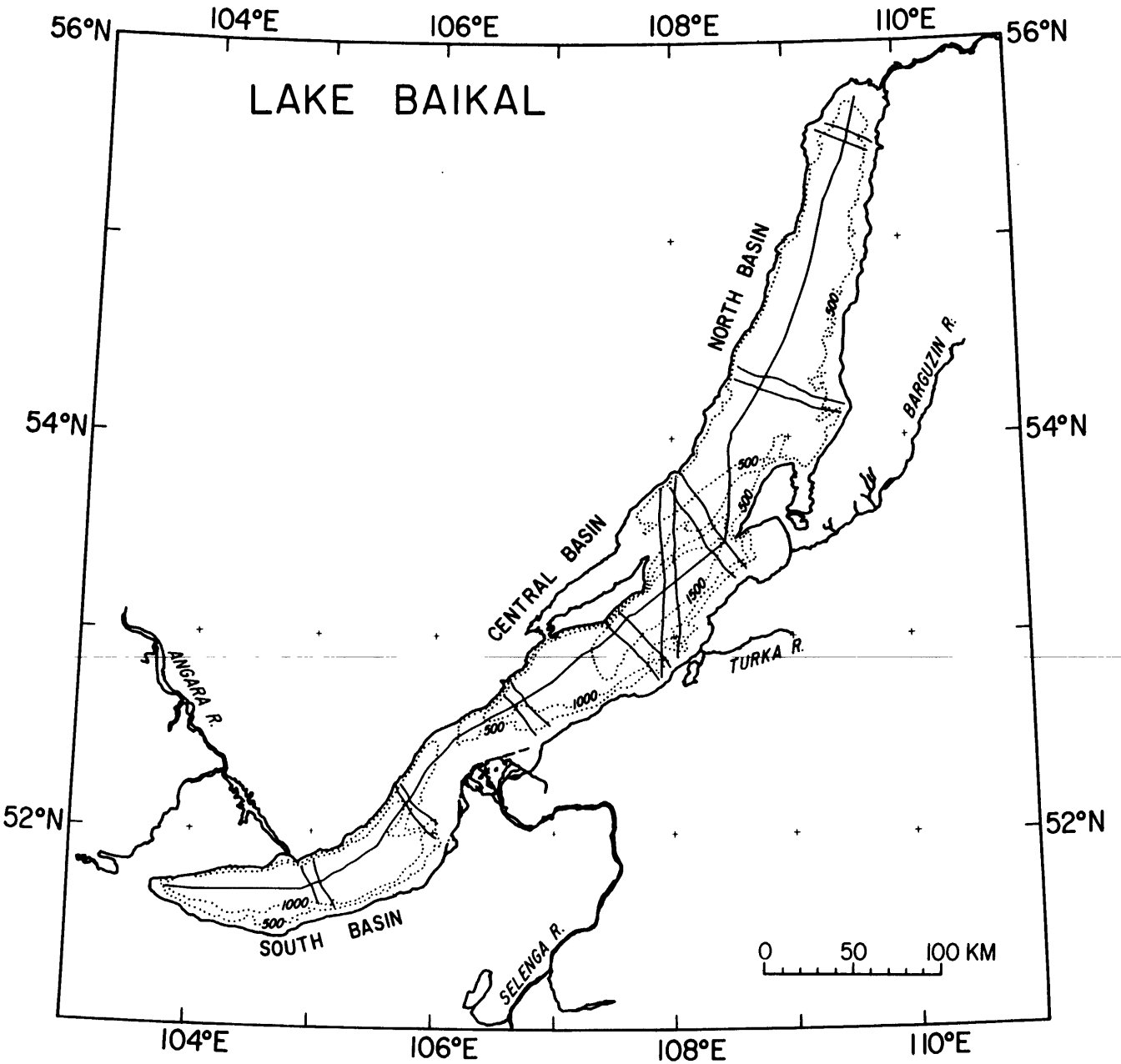
LAKE BAIKAL
56°N
104°E
106°E
108°E
110°E
54°N
52°N
NORTH BASIN
CENTRAL BASIN
SOUTH BASIN
BARGUZIN R.
TURKA R.
ANGARA R.
SELENGA R.
500
1000
1500
0 50 100 KM

Figure 2: Unfiltered (A) and filtered (B) displays of the near-trace from SP 815 - 865 of line 15-6 in the South basin. This display is after demultiplex, edit, and sort, so that the near trace consists of alternating traces of channel 24 and 23. Note the ringy, multicyclic nature of the energy, and the two water-bottom multiple returns that dominate the record at 3.9 and 5.8 s. SP 865 is the trace used for the analyses in figures 3, 8, and 9.

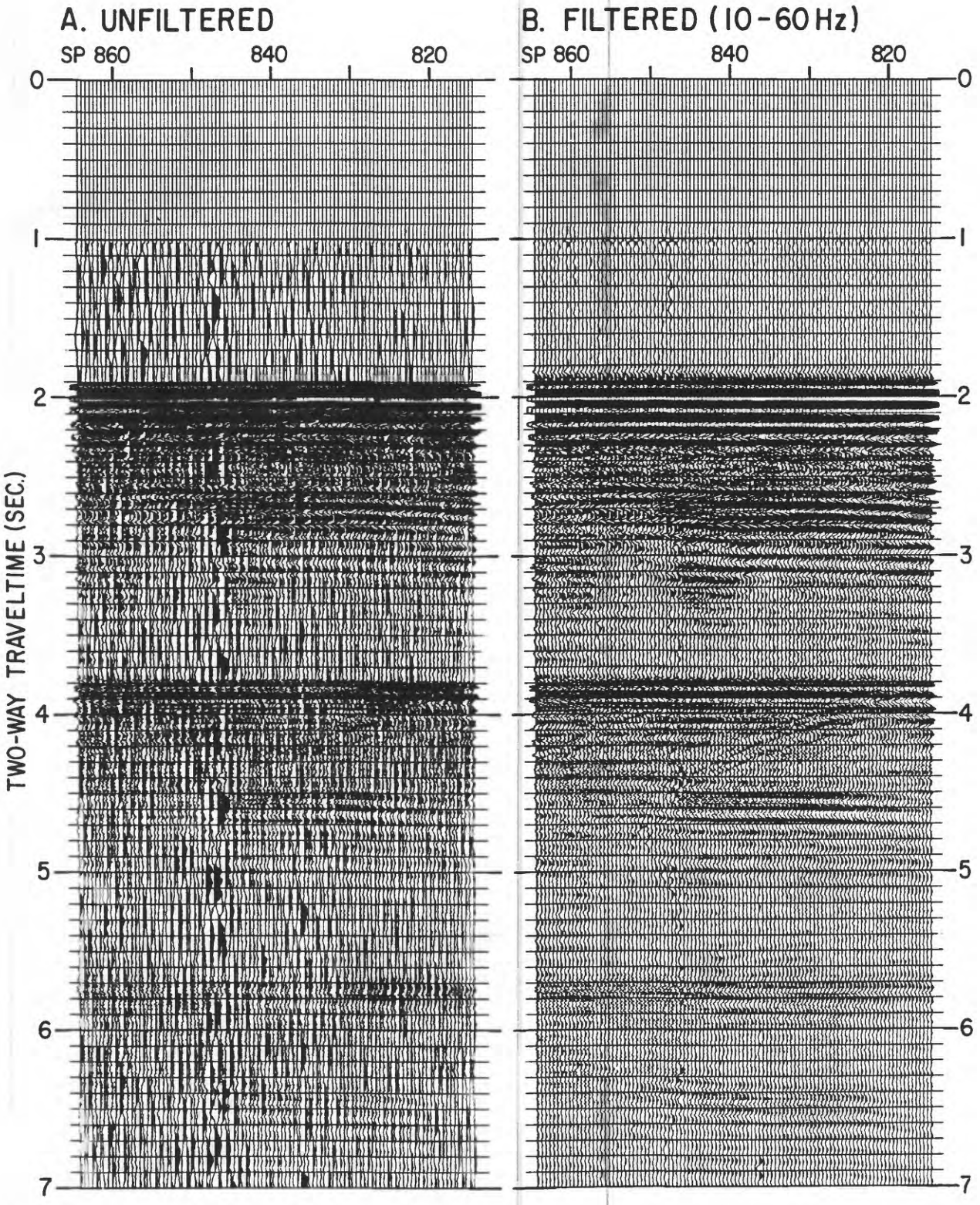
A. UNFILTERED
B. FILTERED (10-60 Hz)
SP 860
840
820
0
1
2
3
4
5
6
7
TWO-WAY TRAVELTIME (SEC.)

Figure 3: Trace display (A) and spectrum analysis (B) of channel 24 from SP 865 (CDP 1750) from line 15-6.

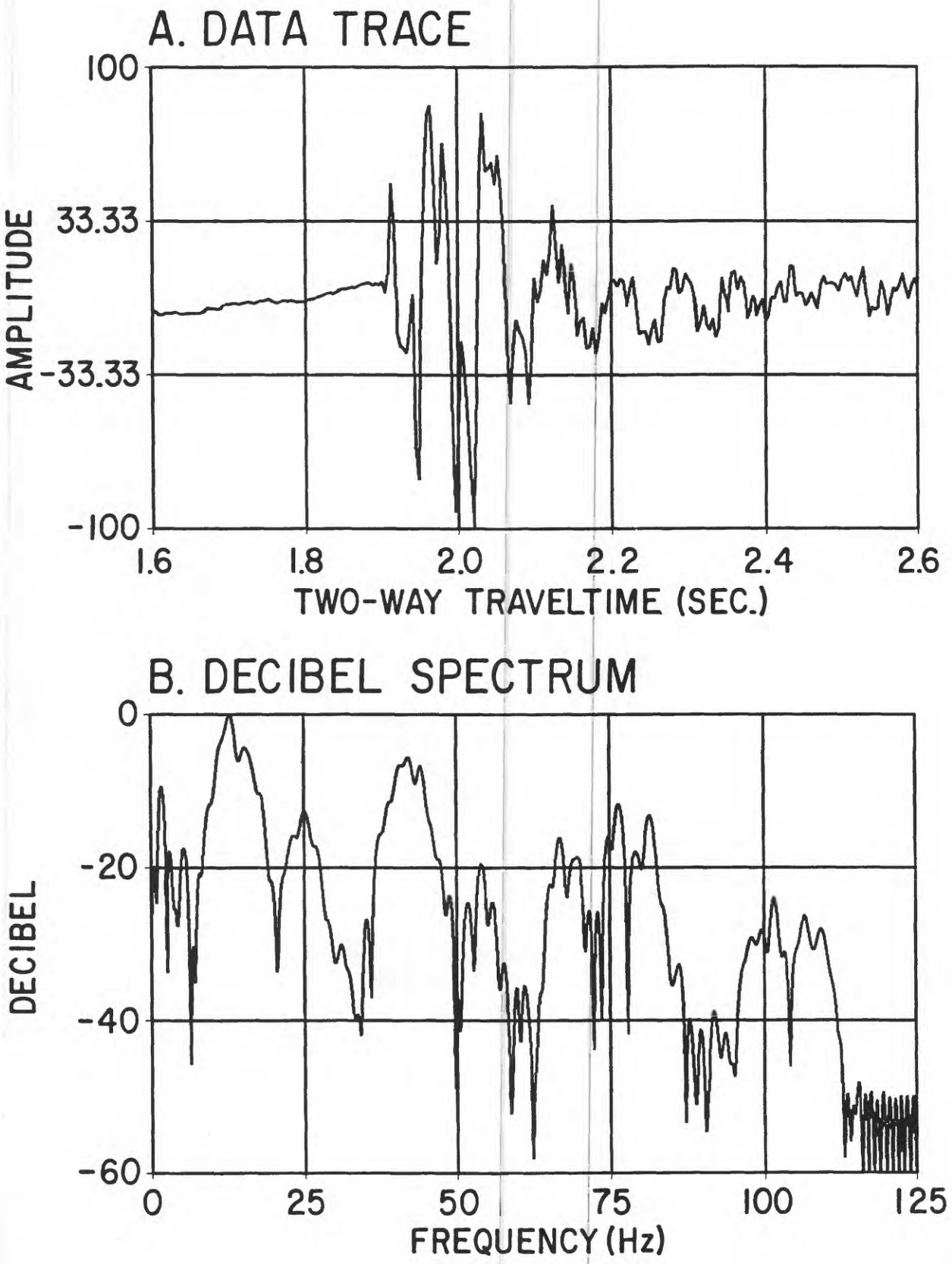
A. DATA TRACE
100
33.33
-33.33
-100
AMPLITUDE
1.6
1.8
2.0
2.2
2.4
2.6
TWO-WAY TRAVELTIME (SEC.)
B. DECIBEL SPECTRUM
0
-20
-40
-60
DECIBEL
0
25
50
75
100
125
FREQUENCY (Hz)

Figure 4: Illustration of the effect of random shot jitter on the near trace of a portion of line 15-6 before (A) and after (B) static shifts to correct the problem. The jitter was caused by random misfirings of the gun that were almost always associated with a programmed firing delay of 1.024 s.

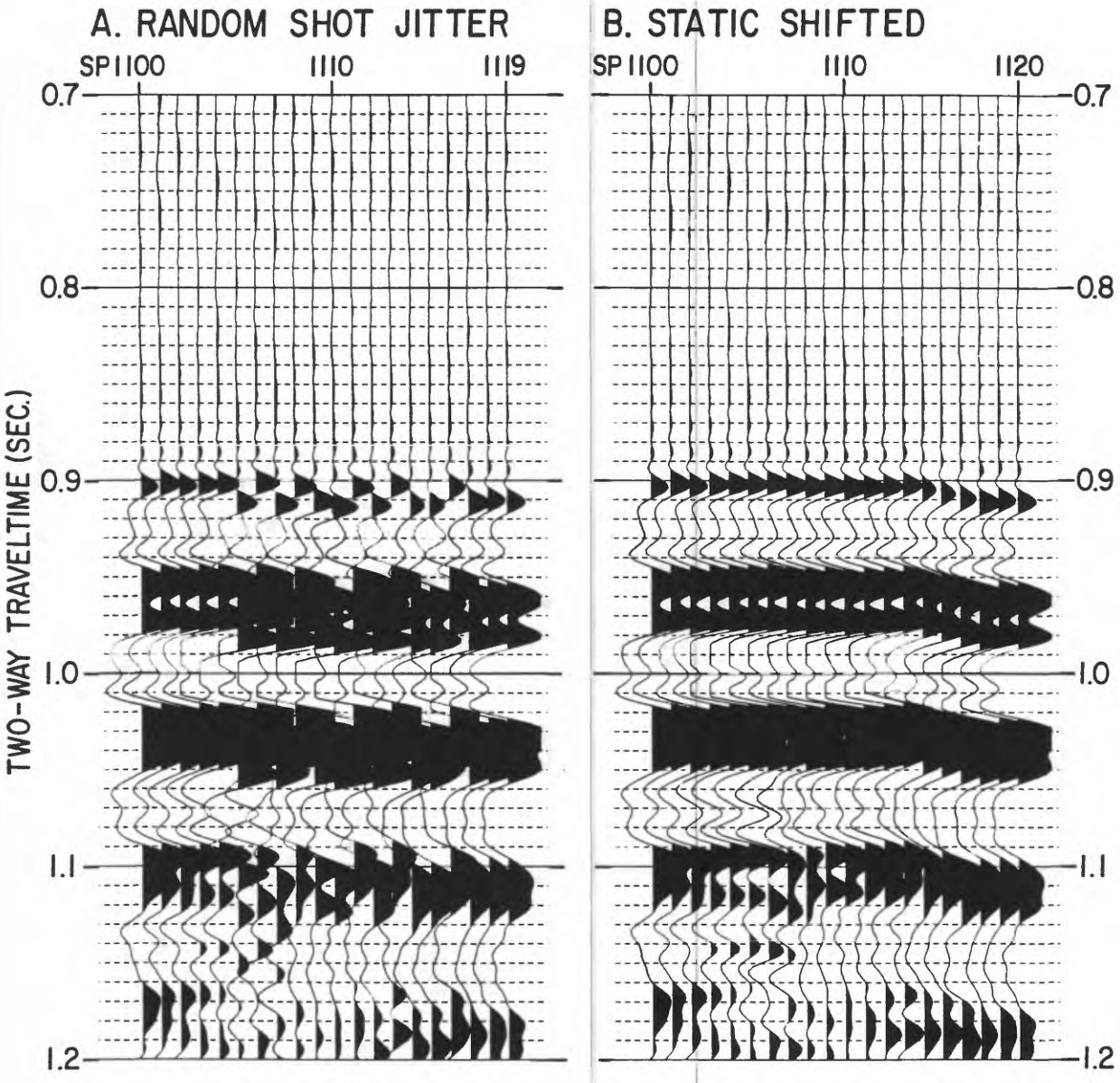
A. RANDOM SHOT JITTER
B. STATIC SHIFTED
SP 1100
1110
1119
1120
0.7
0.8
0.9
1.0
1.1
1.2
TWO-WAY TRAVELTIME (SEC.)

Figure 5: Brute stack of SP 815 - 865 of line 15-6. After edit and sort, the data had only an AGC of 350 ms applied before stack. The reverberatory character of the signal is clearly shown, and the weak signal quality in the deeper section (4 - 7 s) illustrates the blanking phenomenon discussed in the text.

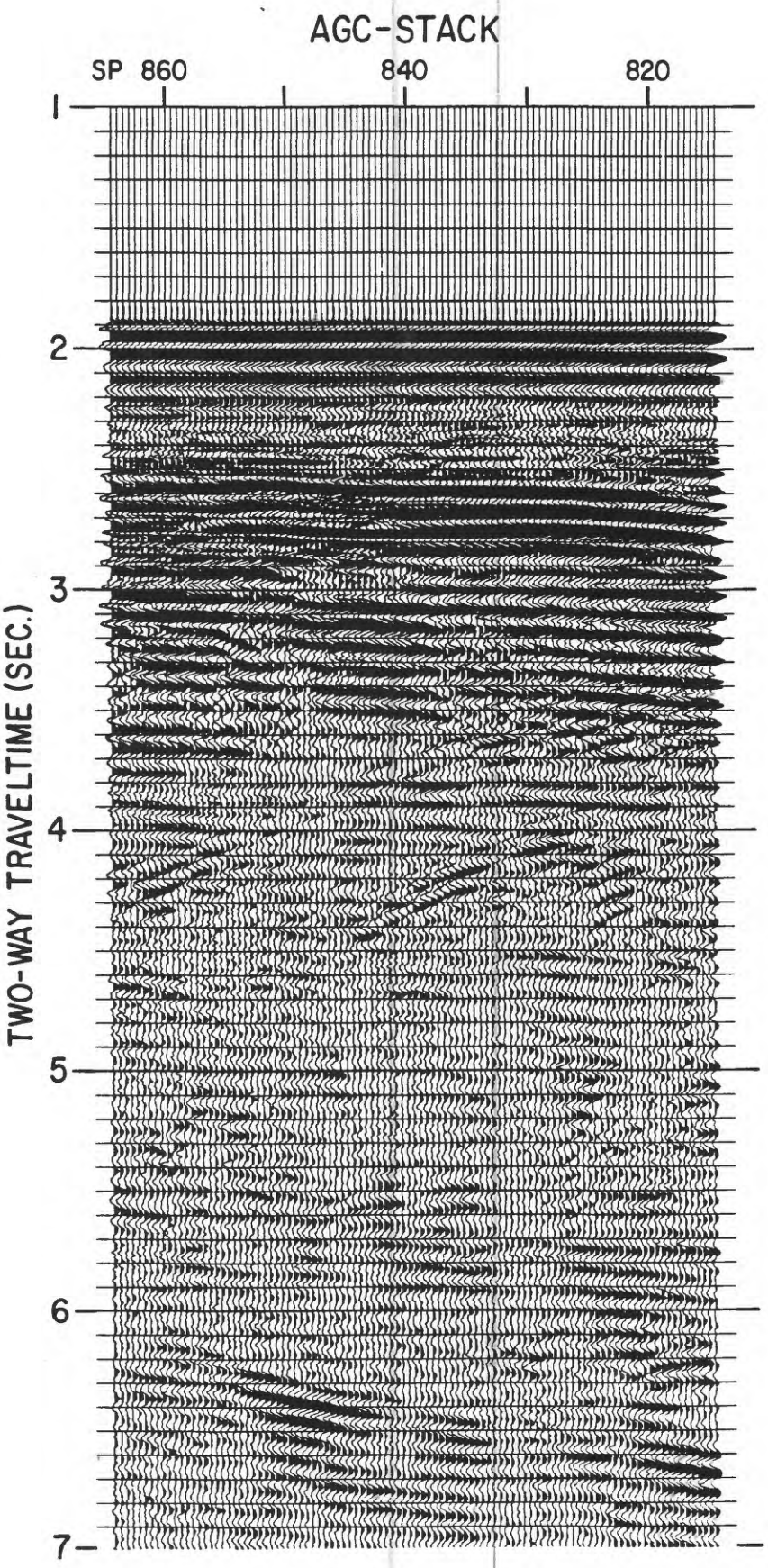
AGC-STACK
SP 860
840
820
1
2
3
4
5
6
7
TWO-WAY TRAVELTIME (SEC.)

Figure 6: Enlargement of the near traces of SP 815 - 839 with a 350-ms AGC applied. The slight offset of adjacent traces reflects alternating channels 23 and 24 in the near-trace display. The signature shows an excellent degree of repeatability between adjacent traces.

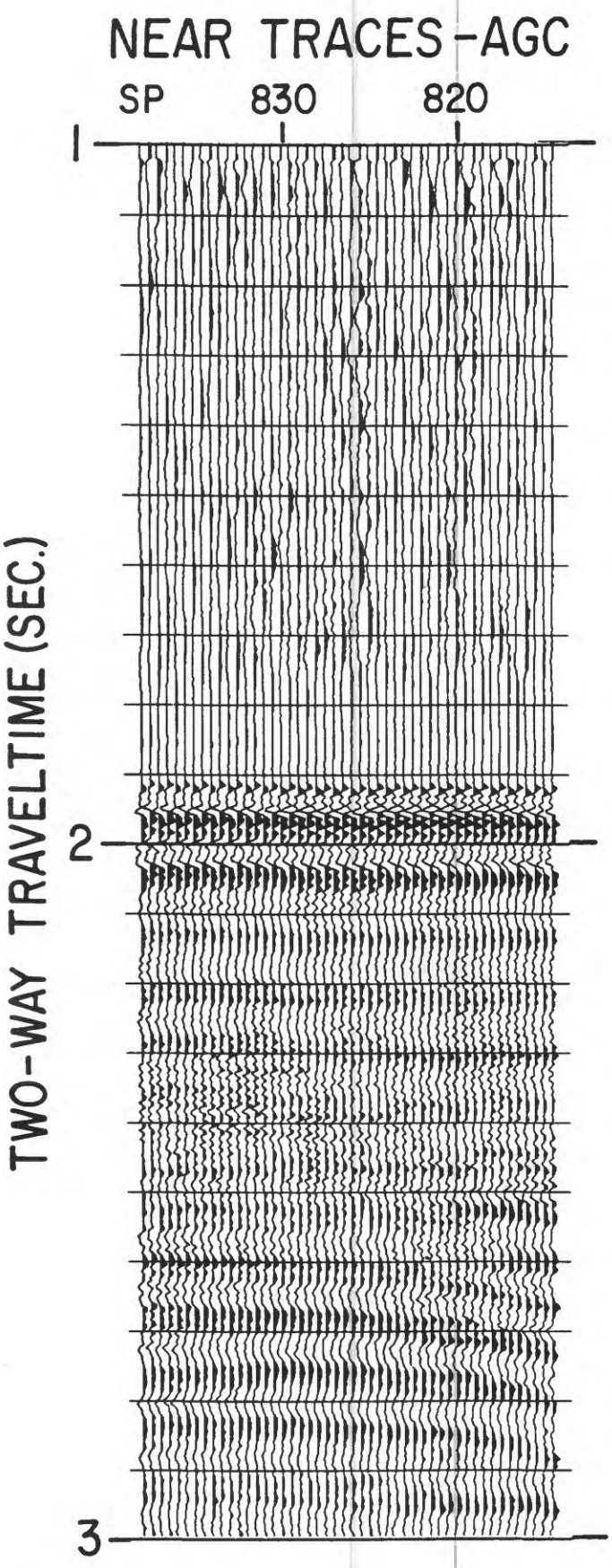
NEAR TRACES-AGC
SP
830
820
1
2
3
TWO-WAY TRAVELTIME (SEC.)

Figure 7: Test stack of SP 815 - 865 using a prestack AGC (350 ms) and a spiking deconvolution (bandpassed at 5 - 70 Hz). This processing shows improved resolution of the data at 2 - 4 s, but the signal quality is still low at 4 - 7 s.

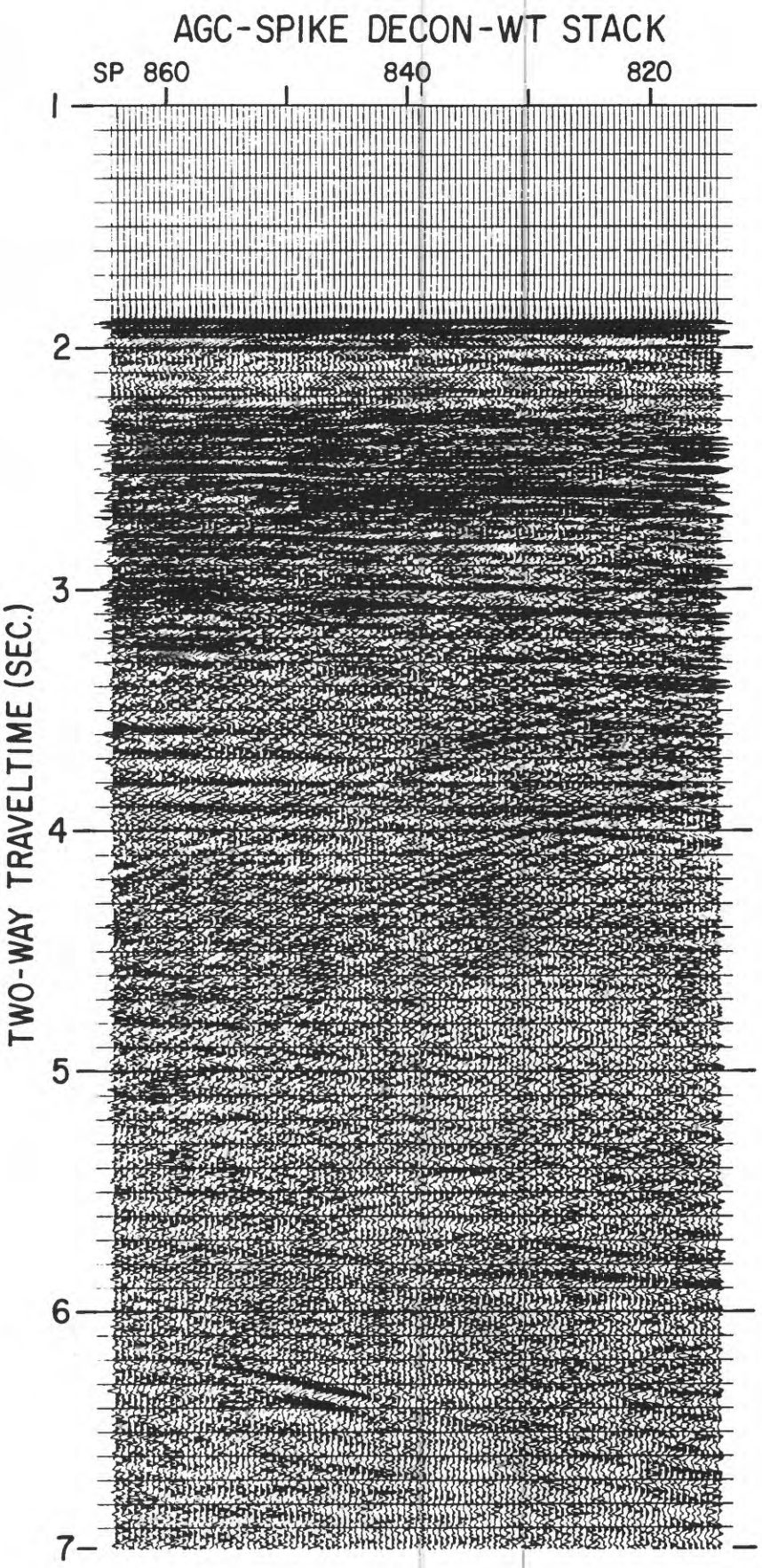
AGC-SPIKE DECON-WT STACK
SP 860
840
820
1
2
3
4
5
6
7
TWO-WAY TRAVELTIME (SEC.)

Figure 8: Extracted wavelet from SP 815 - 865 using a 400-ms design window (A) and a 700-ms design window (B). The respective spectra of the traces are shown in panels C and D.

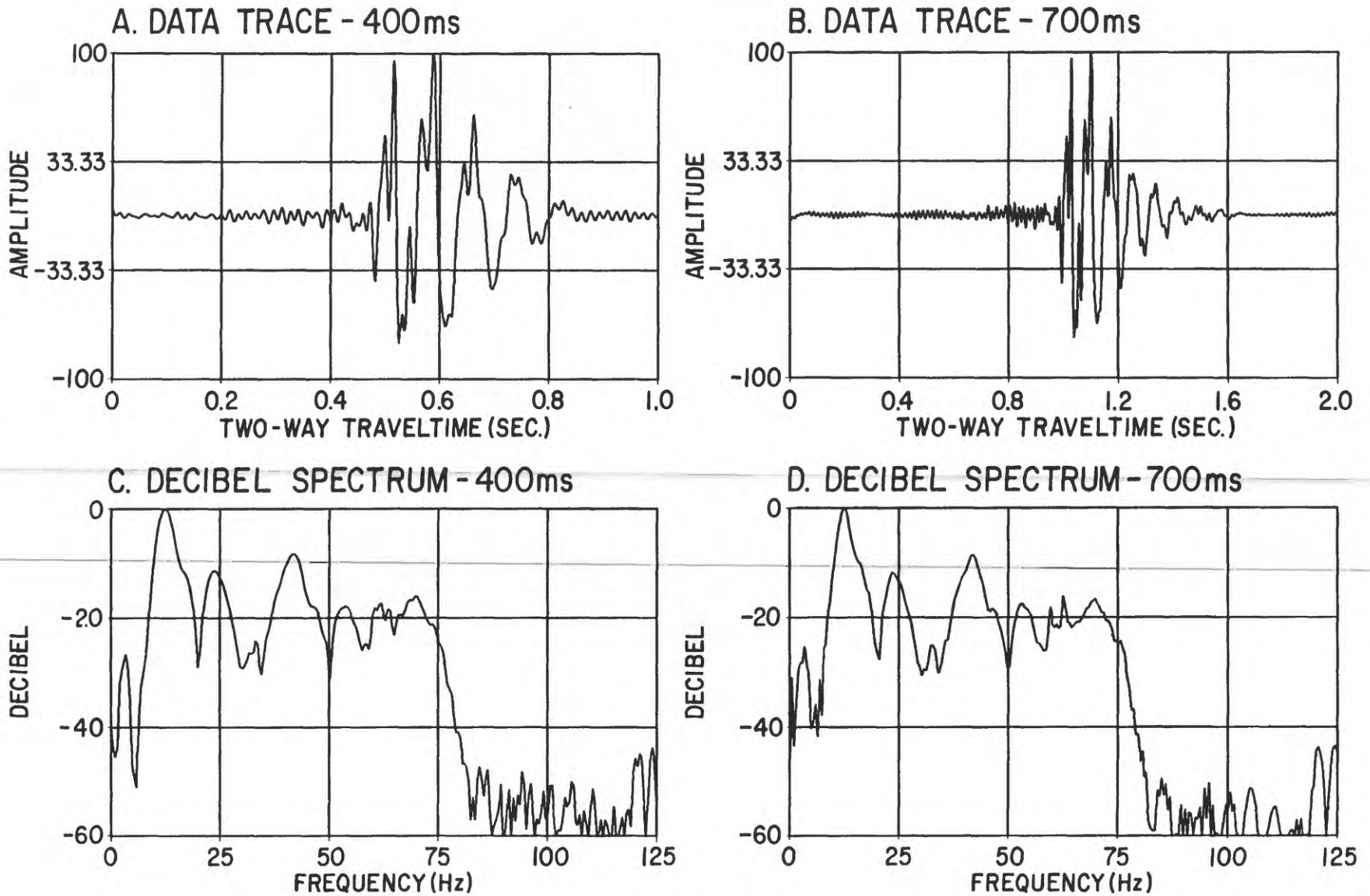
A. DATA TRACE - 400ms
100
33.33
-33.33
-100
AMPLITUDE
0
0.2
0.4
0.6
0.8
1.0
TWO-WAY TRAVELTIME (SEC.)
B. DATA TRACE - 700ms
100
33.33
-33.33
-100
AMPLITUDE
0
0.4
0.8
1.2
1.6
2.0
TWO-WAY TRAVELTIME (SEC.)
C. DECIBEL SPECTRUM - 400ms
0
-20
-40
-60
DECIBEL
0
25
50
75
100
125
FREQUENCY (Hz)
D. DECIBEL SPECTRUM - 700ms
0
-20
-40
-60
DECIBEL
0
25
50
75
100
125
FREQUENCY (Hz)

Figure 9: Trace from channel 24 of SP 865 after wavelet deconvolution using the filter designed from a 400-ms window (A) and from a 700-ms window (B). The respective spectra are shown in panels C and D. Note the similarities in both resulting wavelets and their spectra. The strong negative signal at 1.96 s is the deconvolved water-bottom arrival.

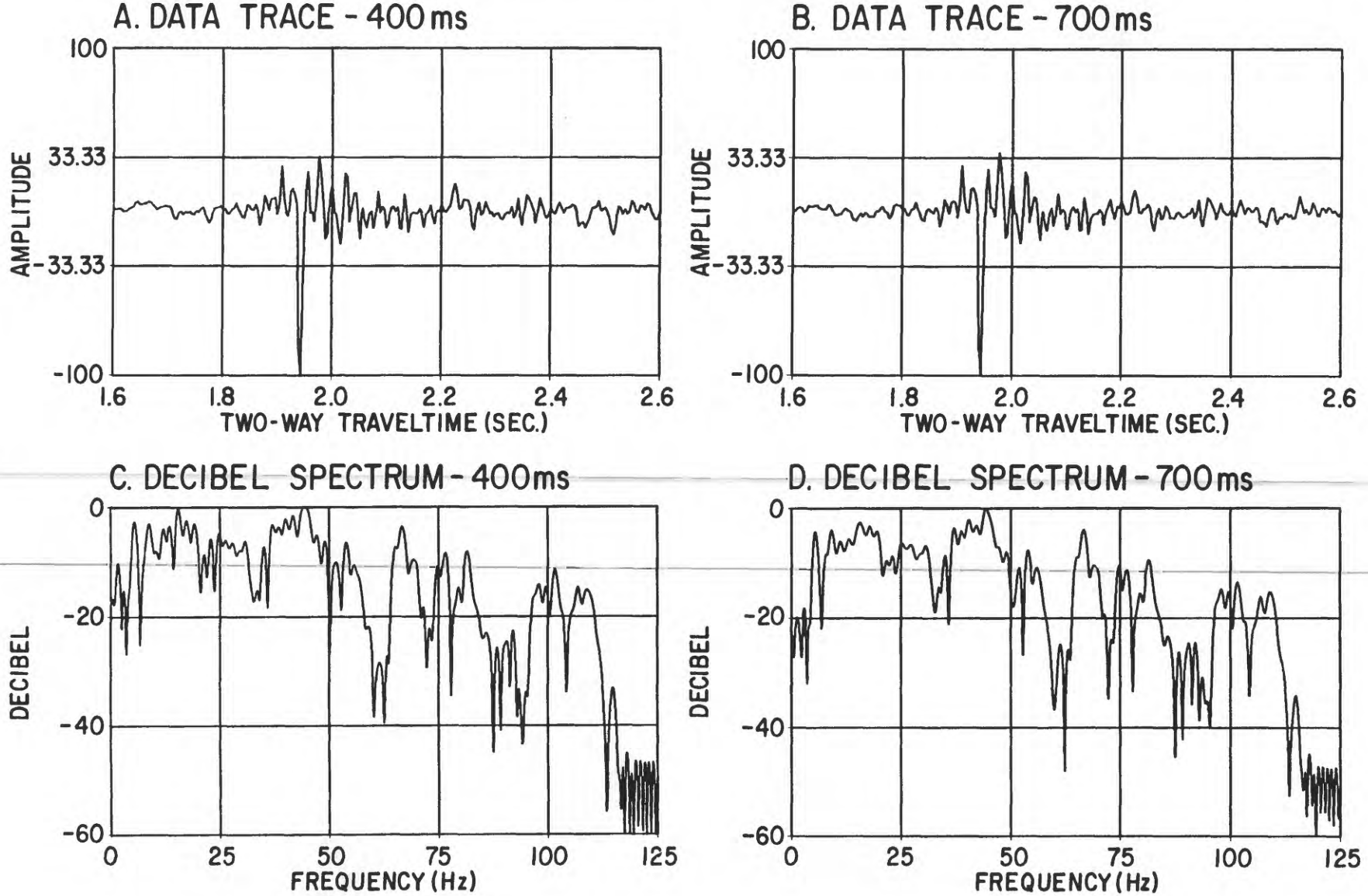
A. DATA TRACE - 400 ms
100
33.33
-33.33
-100
AMPLITUDE
1.6
1.8
2.0
2.2
2.4
2.6
TWO-WAY TRAVELTIME (SEC.)
B. DATA TRACE - 700 ms
100
33.33
-33.33
-100
AMPLITUDE
1.6
1.8
2.0
2.2
2.4
2.6
TWO-WAY TRAVELTIME (SEC.)
C. DECIBEL SPECTRUM - 400 ms
0
-20
-40
-60
DECIBEL
0
25
50
75
100
125
FREQUENCY (Hz)
D. DECIBEL SPECTRUM - 700 ms
0
-20
-40
-60
DECIBEL
0
25
50
75
100
125
FREQUENCY (Hz)

Figure 10 Plots of the near trace of SP 815 - 839 after application of the wavelet filter with 400-ms design window (A) and 700-ms design window (C). The respective panels with AGC applied are shown in B and D. A precursor can be seen at 1.4 - 1.8 s on both of the panels with AGC applied (B and D), but it is much less pronounced on panel D.

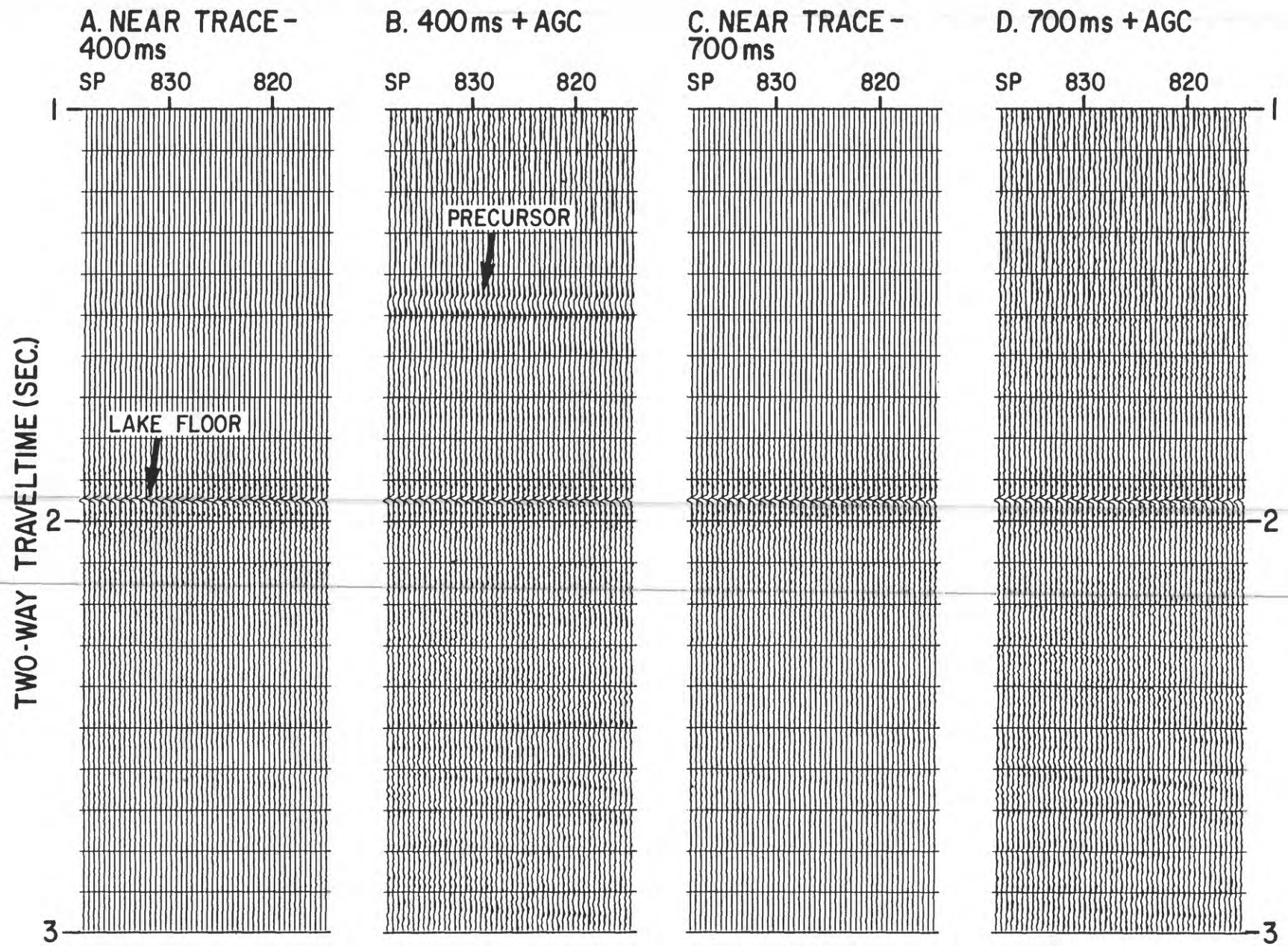
A. NEAR TRACE - 400 ms
B. 400 ms + AGC
C. NEAR TRACE - 700 ms
D. 700 ms + AGC
SP 830 820
PRECURSOR
LAKE FLOOR
TWO-WAY TRAVELTIME (SEC.)
1
2
3

Figure 11 Stack of SP 815 - 865 using prestack wavelet deconvolution followed by an AGC of 350 ms and then stack.

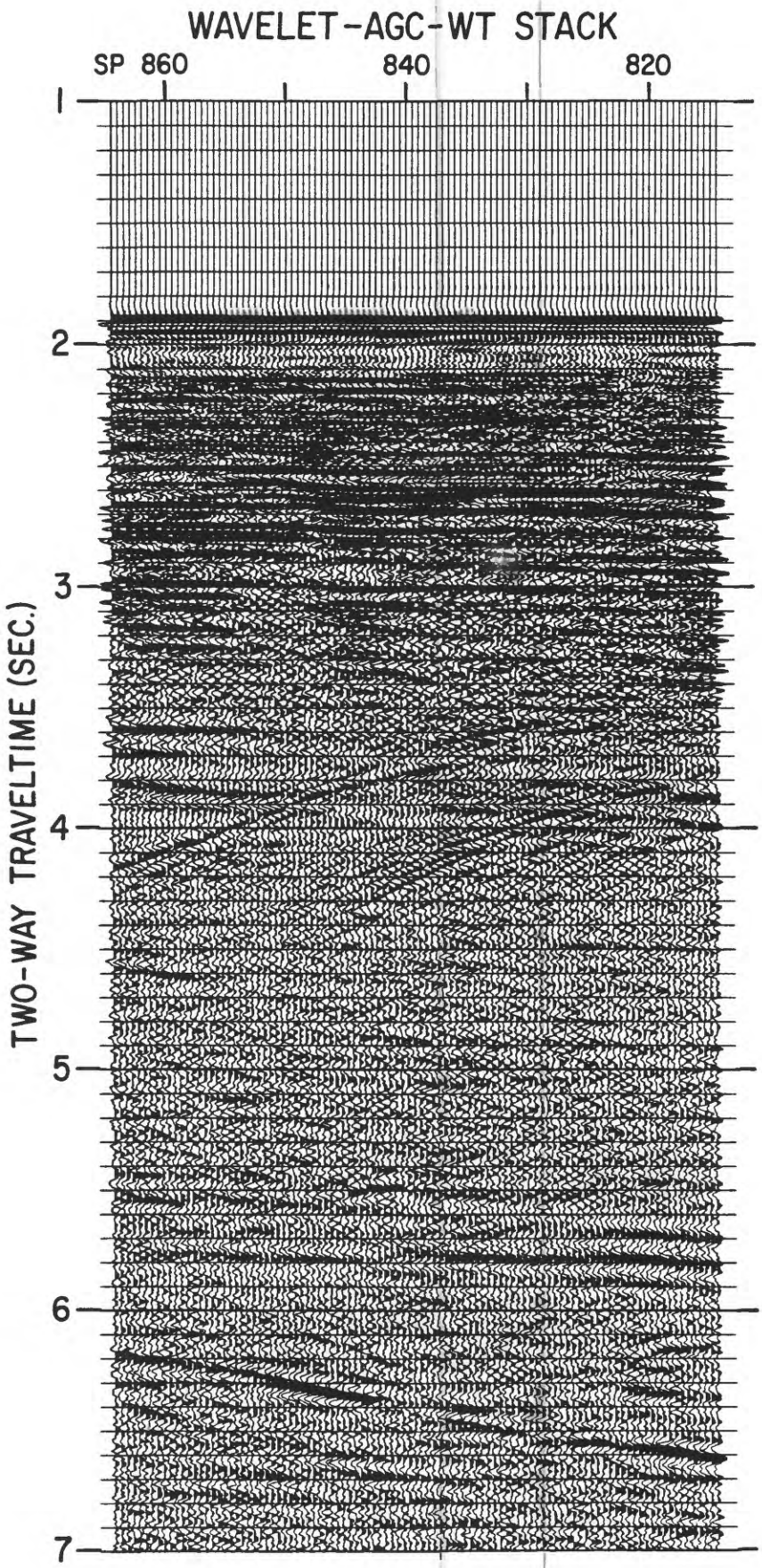
WAVELET-AGC-WT STACK
SP 860
840
820
1
2
3
4
5
6
7
TWO-WAY TRAVELTIME (SEC.)

Figure 12 Stack of SP 815 - 865 using prestack wavelet deconvolution followed by an AGC of 350 ms and a predictive deconvolution, then stack. There is some loss of signal and multiples at 5 - 7 s in this processing scheme compared to that shown in Figure 11, but the overall resolution in the section from 2 - 4 s is improved.

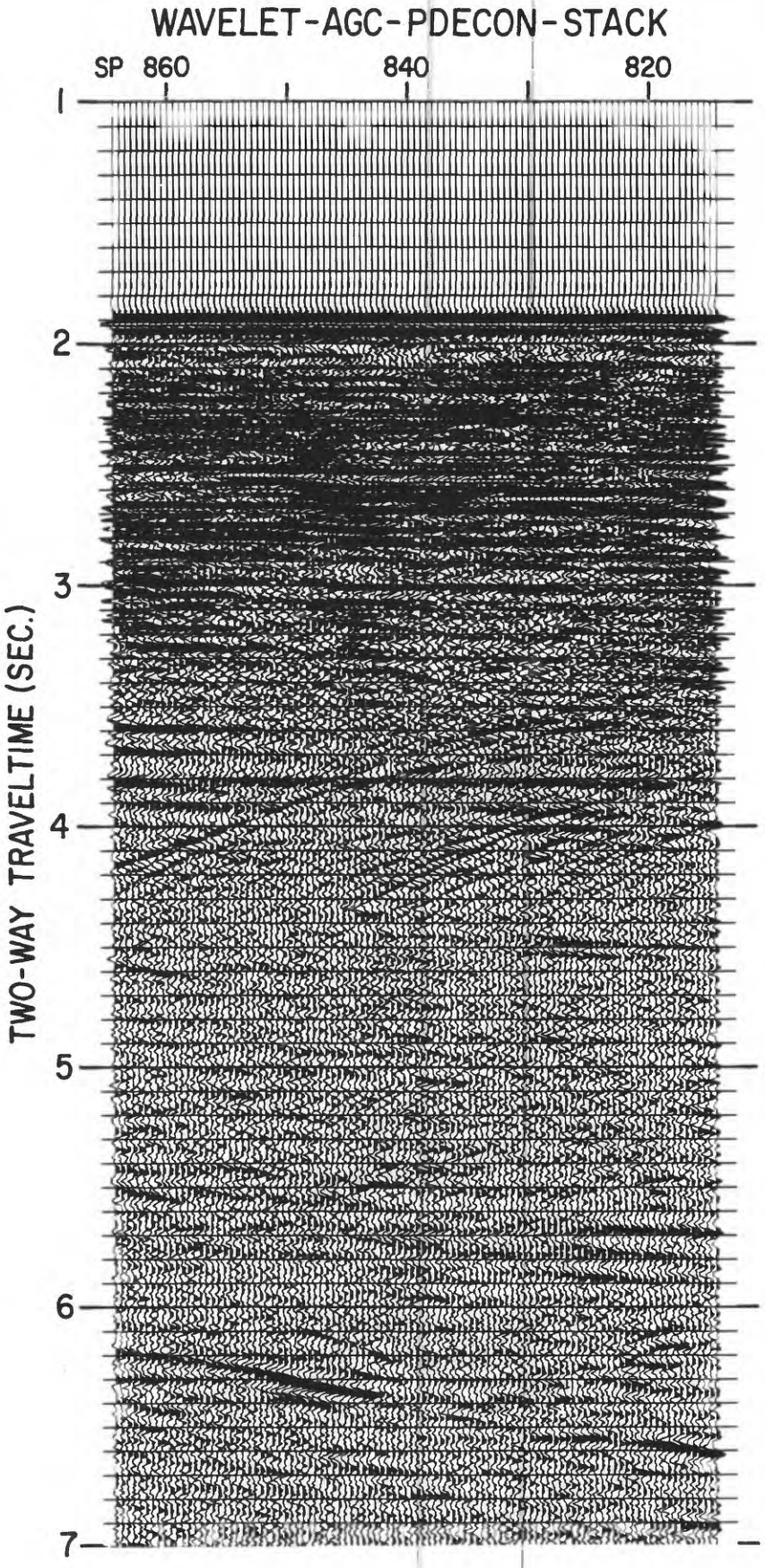
WAVELET-AGC-PDECON-STACK
SP 860
840
820
1
2
3
4
5
6
7
TWO-WAY TRAVELTIME (SEC.)

Figure 13 Stack similar to that used in Figure 12, except that during the stack operation, the far traces are weighted more than the near traces (i.e., weighted stack). The weighted stack has increased the signal strength in the band from 4 - 6 s compared to that of Figure 12.

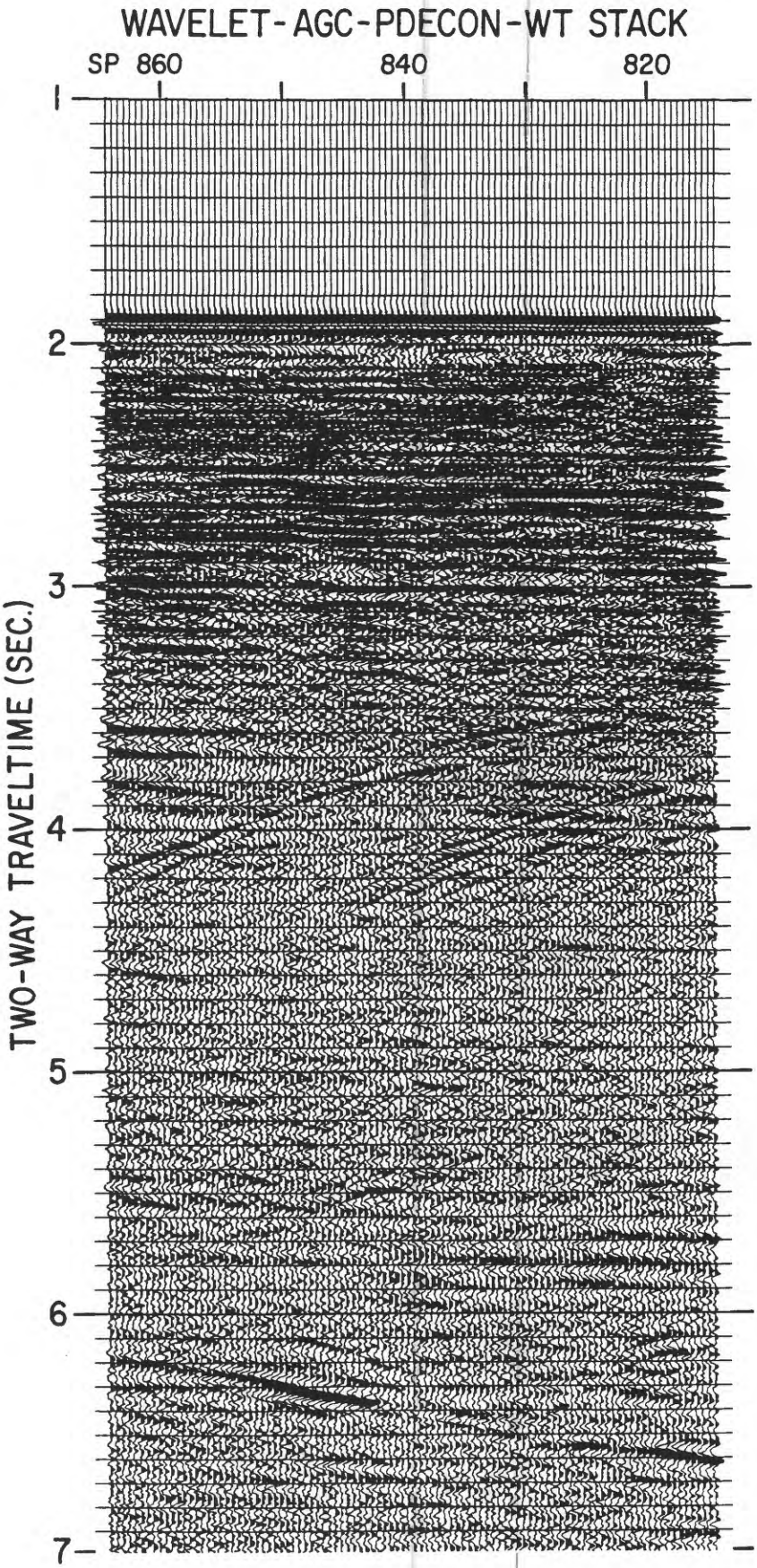
WAVELET-AGC-PDECON-WT STACK
SP 860
840
820
1
2
3
4
5
6
7
TWO-WAY TRAVELTIME (SEC.)

Figure 14 Test stack of SP 815 - 865 using prestack wavelet deconvolution, AGC (1000 ms), spectral whitening, and a weighted stack. Whereas the signal resolution is excellent in the shallow part of the section (2 - 4 s), the overall signal strength, particularly at 4 - 7 s, is less than in the processing using a prestack predictive deconvolution (Fig. 13).

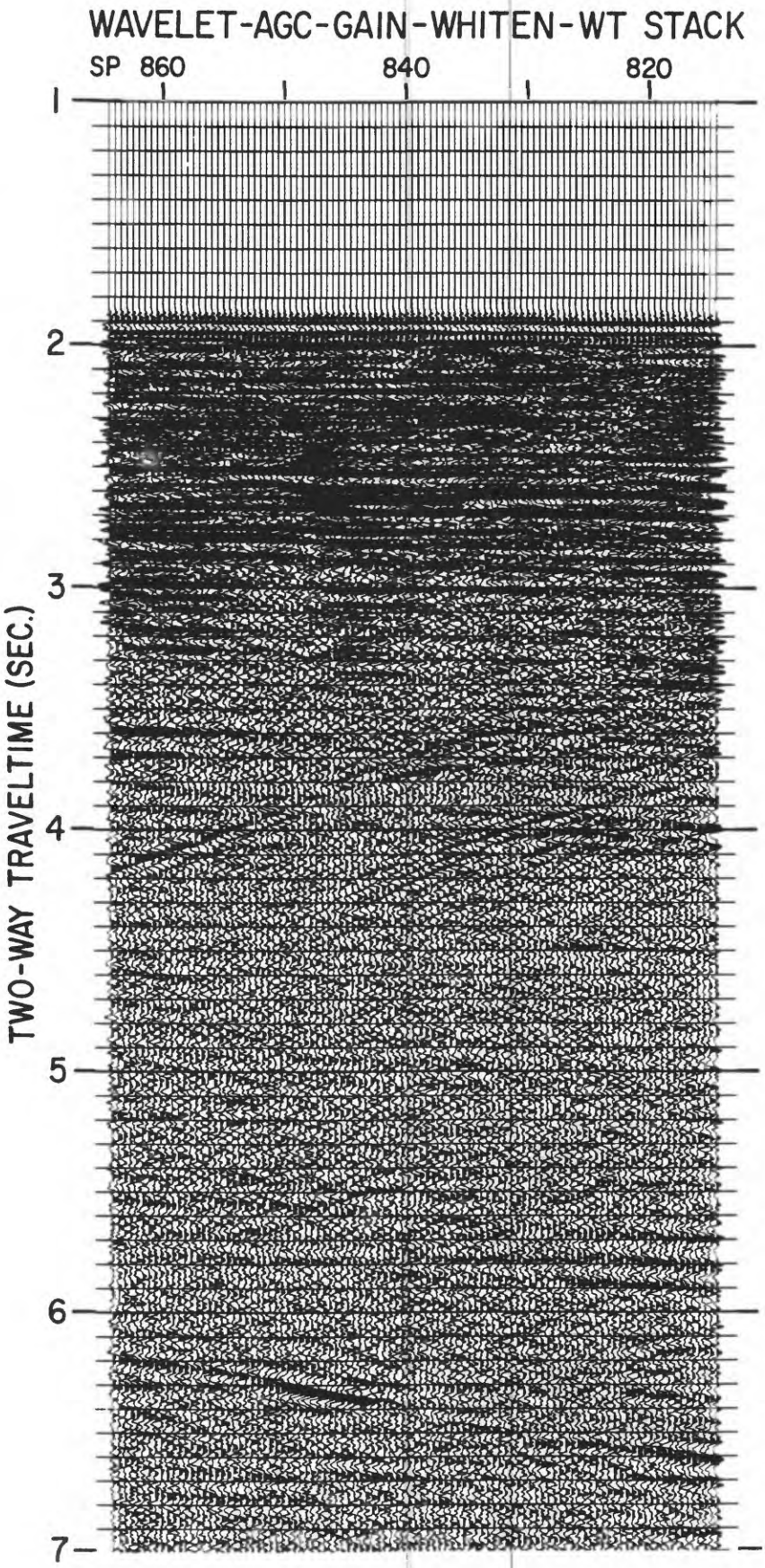
WAVELET-AGC-GAIN-WHITEN-WT STACK
SP 860
840
820
1
2
3
4
5
6
7
TWO-WAY TRAVELTIME (SEC.)

Figure 15 Processing strategy used in the processing of the multichannel data from Lake Baikal.

PROCESSING FLOW

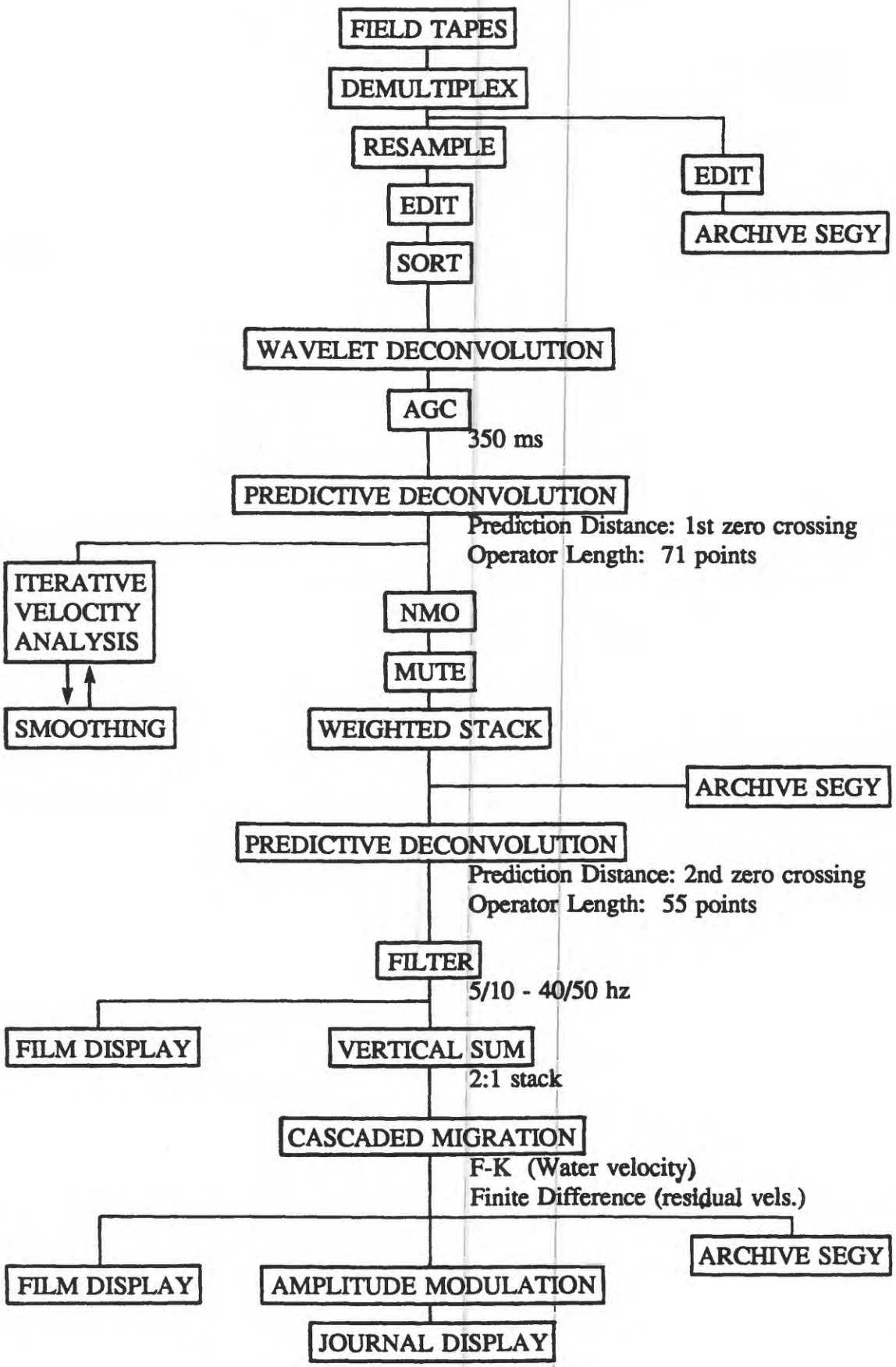

Figure 16 Example of the smoothed RMS (A) and calculated interval (B) velocities used in processing Line 14 from the North basin. Each dot in panel A shows a velocity pick. Regularly spaced dots at 4 - 8 s are the positions of assumed velocities and do not represent real reflectin horizons. Contours are in m/s. Contours are shown on the interval velocity section (B) rather than discrete velocity intervals, since the display would be too complicated. The interval velocities for the deeper (assumed) intervals are shown with arrows.

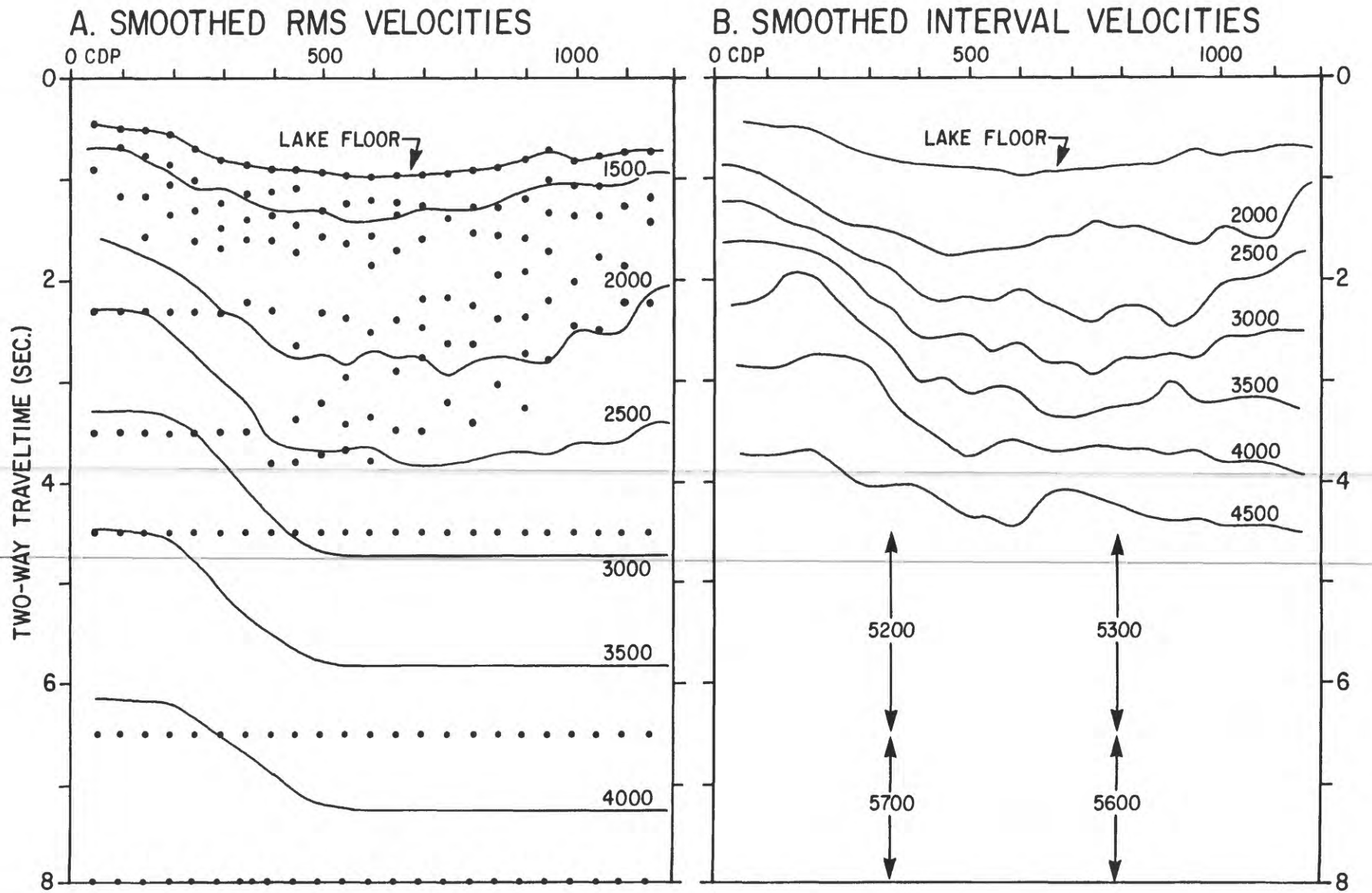
A. SMOOTHED RMS VELOCITIES
B. SMOOTHED INTERVAL VELOCITIES
0 CDP
500
1000
TWO-WAY TRAVELTIME (SEC.)
0
2
4
6
8
LAKE FLOOR
1500
2000
2500
3000
3500
4000
4500
5200
5300
5700
5600

Figure 17 Example of stacked and migrated data from line 8 in the Central basin of Lake Baikal. The signal quality is generally excellent and basement can be identified on the entire profile. Blanking still occurs beneath the level of the first water-bottom multiple, indicating the processing did not fully compensate for this problem.

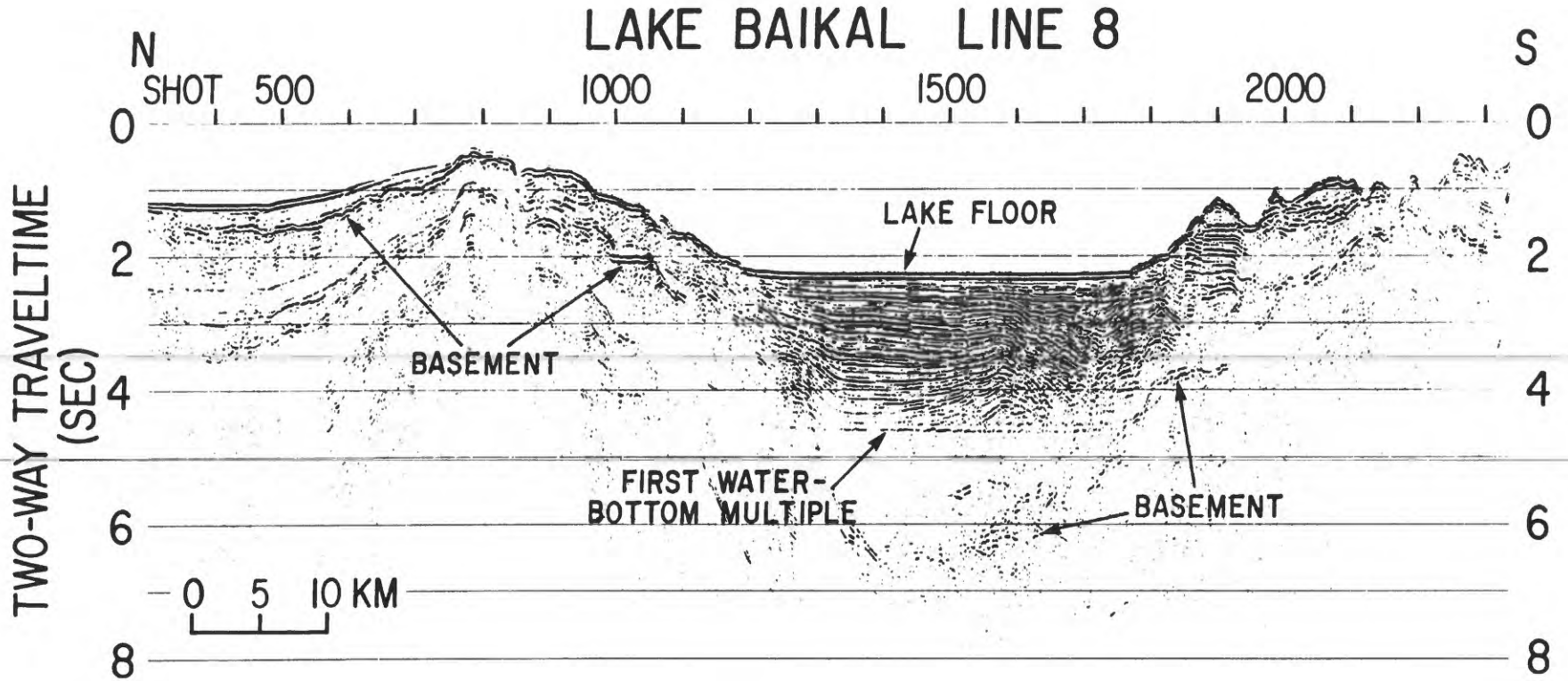
LAKE BAIKAL LINE 8
N
S
SHOT 500
1000
1500
2000
0
2
4
6
8
TWO-WAY TRAVELTIME (SEC)
LAKE FLOOR
BASEMENT
FIRST WATER-BOTTOM MULTIPLE
BASEMENT
0 5 10 KM

Figure 18 Example of stacked and migrated data from line 6 in the Central basin of Lake Baikal. The signal quality is not very good on this profile, and the first water-bottom multiple has created a zone of blanking in which no primary energy can be identified. Basement is not imaged anywhere on this profile.

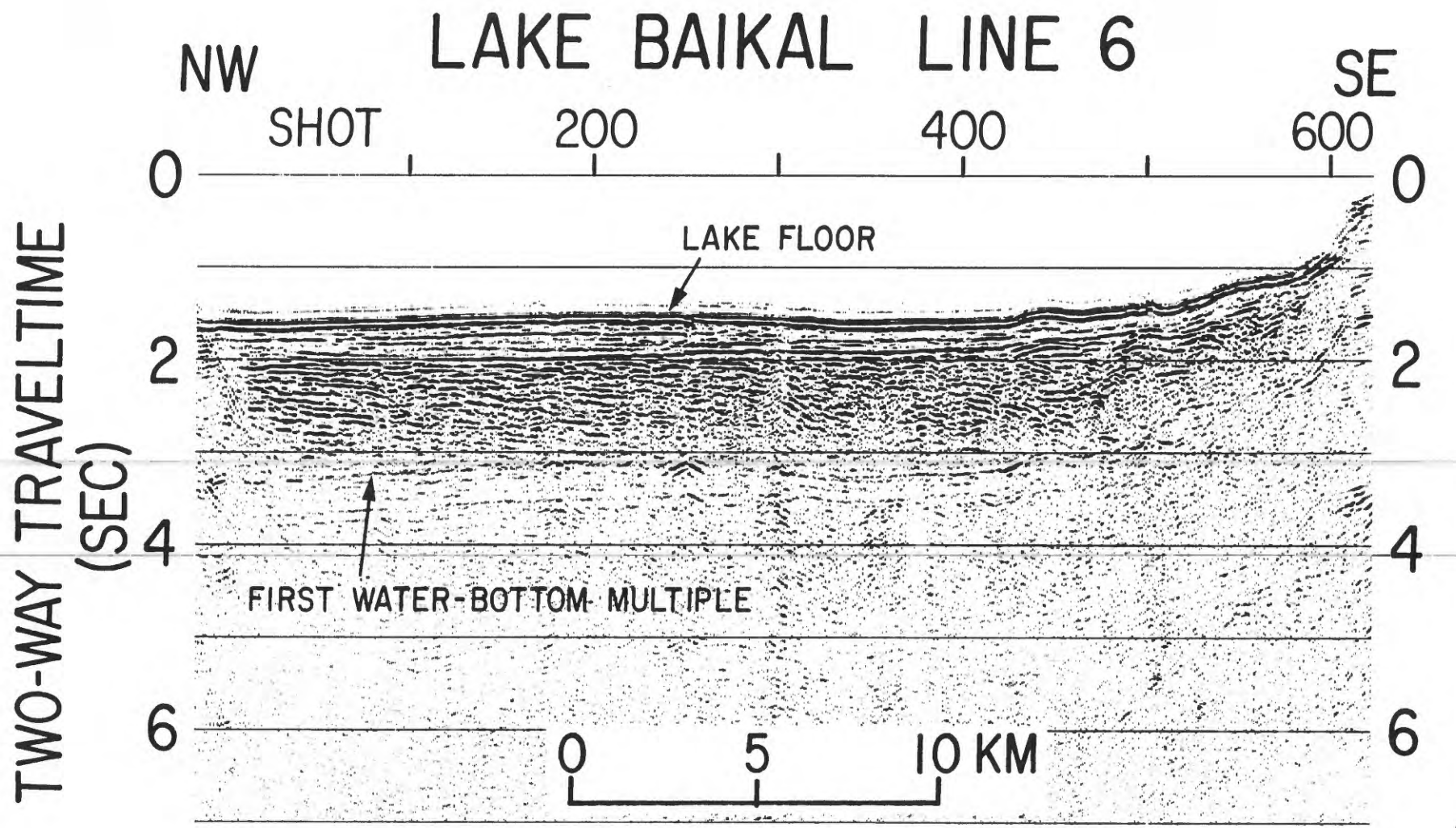
LAKE BAIKAL LINE 6
NW
SE
SHOT
200
400
600
0
2
4
6
TWO-WAY TRAVELTIME (SEC)
LAKE FLOOR
FIRST WATER-BOTTOM MULTIPLE
0
5
10 KM

PLATE 1 1989 Multichannel tracklines in Lake Baikal. Solid lines show tracklines with ticks every 100 shots. Starting and ending shots and even 500 shot-point intervals are annotated. Line numbers are bold type. Dots indicate navigation control points during profiling. Line 15, along the axis of the lake, is broken into 8 segments; black bars on either side of the tracklines indicate the breaks between adjacent segments. SD - Selenga Delta. OI - Ol'khon Island.